NUMERICAL INVESTIGATION OF FLOW FIELD ON A CENTRIFUGAL SLURRY PUMP

Thesis submitted in partial fulfilment of the requirements for the award of degree of

Master of Engineering

in

CAD/CAM & ROBOTICS

Thapar University, Patiala

By:

Chander Kant Susheel

Roll No. 80681005

Under the supervision of:

Mr. Satish Kumar

Lecturer, MED

JUNE 2008

MECHANICAL ENGINEERING DEPARTMENT

THAPAR UNIVERSITY

PATIALA – 147004

CERTIFICATE

I hereby certify that the work which is being presented in the thesis entitled, **"*Numerical investigation of flow field on the centrifugal slurry pump*"**, in partial fulfillment of the requirements for the award of degree of Master of Engineering in CAD/CAM and Robotics submitted in Mechanical Engineering Department of Thapar University, Patiala, is an authentic record of my own work carried out under the supervision of **Mr. Satish Kumar**.

The matter presented in this thesis has not been submitted for the award of any other degree of this or any other university.

(Chander Kant Susheel)

This is to certify that the above statement made by the candidate is correct and true to the best of my knowledge.

(Satish Kumar)
Mechanical Engineering Department
Thapar University
Patiala

11/7/08

(Dr. S. K. Mohapatra)
Professor & Head
Mechanical Engineering Department
Thapar University
Patiala

(R.K.SHARMA)
Dean(Academic Affaris)
Thapar University,
Patiala.

ACKNOWLEDGMENT

I would like to extend my gratitude to the following who and which made it possible for me to survive the thesis period with 'flying colors'. This thesis has been an inspiring, very challenging, but always interesting and exciting experience. In first place I would like to express my sincere gratitude to my guide Mr. Satish Kumar, lecturer, Department of Mechanical Engineering, Thapar University, Patiala for acting as supervisors and giving valuable guidance, for the patience, encouragement, many fruitful discussions, and never giving up on me.

I also thanks to entire faculty and staff of Department of Mechanical Engineering, Thapar institute of Engineering & Technology, Patiala for their help, Inspiration and moral support, which went a long way in successfully completion of my thesis.

(CHANDER KANT SUSHEEL)

ABSTRACT

The flow field in centrifugal slurry pumps is influenced by fluid rotation and curvature, which are highly turbulent and unsteady. Due to separation and recirculation of flow, it became very complex. In order to study these changes in the flow field lots of work has been done previously, both experimentally and numerically. With new CFD software's the analysis has become easier and helped in improving the efficiency of the pumps. In the present study numerical investigation of flow field inside the centrifugal slurry pump is done. For this purpose a design code has been written. Thereafter, output of the program has been used for modeling of impeller of pump using Ansys-CFX, CFD software. Also study of variation of different parameters, such as pressure and velocity, in the flow field of centrifugal pump impeller in single and two phase flow conditions is done. The effect of flow rate on the flow field is also investigated. The pressure variation from inlet to outlet of the impeller along the streamwise location is also studied. Performance characteristics of the pump are also developed. It is observed that head of the pump decreases with increasing flow rate and the concentration of the sand in the fluid. Input power required at the shaft also increases as concentration increases. But there is not much of change in the efficiency of pump with changing concentration.

CONTENTS

LIST OF FIGURES

LIST OF TABLES

NOMENCLATURE

SYMBOLS	STANDS FOR
N	Speed of the pump in rpm
Q	Discharge in m^3 / sec
H	Net head in m
N_s	Specific speed
P_o	Output power
$P_{in,}$	Input power
P_{sh}	Shaft power
ρ	Density of fluid
g	Acceleration due to gravity
η_h	Hydraulic efficiency
η_o	Overall efficiency
η_m	Mechanical efficiency
T	Torque transmitted by the shaft
F_s	Allowable shear stress
D_{sh}	Shaft diameter
D_{hb}	Hub diameter
C_A	Axial Velocity at entry of impeller
C_2	Absolute Velocity at inlet of the blade
C_3	Absolute Velocity at eye of the blade
D_1	Diameter at the inlet of the blade
b_1	Breadth of the blade at the inlet
u_1	Blade velocity at inlet
u_2	Blade velocity at outlet
β_1	Blade inlet angle

H_r	Total head generated
Z	Number of blades
C_{1m}	Meridional flow velocity at inlet of impeller
C_{2m}	Meridional Flow Velocity at impeller outlet
B_2	Width of blade at Outlet
r_1	Outer radius of the blade
ω	Angular velocity of impeller
F_s	Sear stress depending on the type of material
ε	Turbulence eddy dissipation (the rate at which the velocity fluctuations dissipate)
k	Turbulence kinetic energy per unit mass
B	Sum of body forces
μ_{eff}	Effective viscosity accounting for turbulence
μ_t	Turbulence viscosity
w	Turbulence frequency
F_2	Blending function
S	Invariant measure of the strain rate
t	Time in seconds
u	Component of velocity in x-direction
v	Component of velocity in y-direction
B_2	Width of blade at outlet
ΔH	Net Positive Suction Head (NPSH)
p	Pfleiderer's coefficient

` CHAPTER 1
INTRODUCTION

Centrifugal pumps are prevalent for many applications in the industrial or other sectors. Nevertheless, their design and performance prediction process is still a difficult task, mainly due to the great number of free geometric parameters, the effect of which cannot be directly predicted. The flow inside the impeller of the centrifugal pump is extremely difficult to predict because of the separation and recirculation of the flow at the inlet and exit. The curvature of the blades has great influence on the flow structure. The flow structure became more complex with the addition of the solid particles in the fluid. This gives rise to another field of multiphase fluid system. These types of pump, called centrifugal slurry pumps, are extremely used in pipeline transportation system, mining industries, petroleum industries, sewage and sump services etc.

Multiphase fluid systems contain more than one phase, and at least one of them being a fluid. The disperse phase may consist of solid particles, gas bubbles, or liquid droplets when the continuous phase is a liquid. The dynamics of multiphase systems comprises of mass, energy, charge, and momentum transports in these systems. Multiphase systems might have gas-solid particles, gas- liquid droplets, liquid-gas bubbles, liquid- liquid droplets, and liquid-solid particles. There are two methods of approach to the dynamics of multiphase systems: firstly, considering the dynamics of a single particle and then extending it to a multiphase system in an analogous fashion. Secondly, investigating the continuum mechanics of single -phase fluids, then using a similar way to explain what happens in the presence of particles. Generally, the shapes of the particles in multiphase systems are not spherical. To make irregular shapes as ideal, particles are assumed to be as spherical. Small liquid droplets attempt to be spherical because of the surface tension phenomenon. If field effect or gravity comes into picture, droplets tend to have shapes that cause minimum potential or smallest resistance to flow.

The factors that affect the solid-liquid flows can be stated as follows: particle- particle interaction, the virtual mass affect, particle inertia, crossing -trajectories effect, drag,

turbulence, and the Magnus effect. If the volumetric concentration of solids is less than 0.3%, the particle-particle interactions are considered to be negligible for spherical particles. When having neutrally buoyant particles, velocity of solid phase and velocity of fluid are accepted as equal in the laminar flow regime even if the concentration of solids is large. Particle interactions can be neglected in dilute slurries. Particle behavior in gas-solid flows depends on:

1. Drag force (due to slip velocity).
2. Lift force (because of the rotation of particles and gas velocity gradient).
3. Gravity force (important for horizontal flow).
4. Particle- particle and particle- wall interactions.
5. Electrostatic forces.

Transportation of solid- fluid mixtures finds many uses in industry; such as food processing and sterilization operations. Suspension flows have largely been used in the transportation of solid raw materials, products, solid wastes and sludges, mining and beneficiation plants. Also circulating fluidized beds, hydraulic transportation of minerals and ores, mining and beneficiation plants, mineral and chemical process industries, chemical and fossil energy applications are some of the other examples of slurry flows. If the flows of such kind of mixtures are not understood well enough, it causes some inefficiencies in the use of the equipment or some problems in the operations depending upon the improper design of them. Different flow patterns can be observed in liquid-solid flows as in the other flow systems. Geometry of the system, operating conditions and physical properties of the fluids, altogether affect the flow pattern. Internal flow pattern plays a role in the performance of a system. By knowing the local concentrations, this phenomenon could be understood. Also pressure drop, corrosion, erosion, and power requirements depend on the concentration of solids in slurry systems. Estimation of the pressure drop in slurry pump design is not easy because of the complexity of the process. Shape and size distributions of solid particles are significant factors in predicting the pressure drop through a pump, which is very important in the design of hydro-transport systems. On the other hand, restricted amount of experimental data makes difficult to get valid estimations for large-scale plants.

Pressure drop increases when the solid particles are present in the fluid, since the velocity between the solid particles (interstitial velocity) is higher than the superficial velocity. Another reason yielding higher pressure drops in the presence of solid particles is because of the higher turbulence in solid -liquid flow than that in single- phase flow, and due to the increase in the form drag. The application of upward liquid-solid flows in hydraulic transport in industry, require the operating velocity being high enough to keep the continuous flow of solids. Nonetheless, high velocity causes excess energy losses and sometimes wears. In the hydraulic transportation of settling solids in horizontal pumps, the transport velocities smaller than the suspending velocity are used at most of the time, to be more economical. Slurry flow in pumps is different from the homogeneous liquid flow in several aspects: for the latter case, the nature of the flow depends on the physical properties of the fluid, while for the former case two different types of flow affect the system:

i) Homogeneous slurries: These slurries have uniform solid particle distribution in liquid medium. Size of the particles is very small (fine) and solid concentration is high.

ii) Heterogeneous slurries: Distribution of the solid particles is not uniform.

There are concentration gradients through the vertical axis of a pump, even at high flow rates, since the solid and fluid phases keep their identities so that particle- fluid interactions may be significant. Particle sizes are larger and solid concentration is lower than the homogeneous slurries. To be able to predict the pressure gradients for slurries flowing in horizontal pumps more correctly, slurries can be divided into two main groups: settling and non-settling. In non-settling slurries, the mixture is assumed to behave as a homogeneous fluid and the settling tendency of solid particles could be neglected. However, settling slurries are considered as two- phase mixtures and settling velocity of solids cannot be ignored. Four flow patterns can be defined for slurries: stationary bed, sliding bed, heterogeneous suspension, and pseudo -homogeneous suspension. Flow velocity well above the terminal velocity of particles prevents the settling of solids in vertical pipelines, while turbulence prevents the settling of solids in horizontal pipelines.

CHAPTER 2
LITERATURE REVIEW

Miner, S. M. [1] [1997] has calculated numerically the flow field and pressure field within the rotor of an axial flow pump. Velocity and pressure profiles were developed on both sides of the impeller. It is observed that the value of tangential velocity increases from the centre line to the outer radius. The axial velocity profile shifts towards the outer radius because of the presence of nose on the hub. The use of coarse and fine mesh does not show significant difference in the values, thus even coarser mesh can be used.

Murugan, D. M. et al[2] [1997] have observed flow using LDV system in the exit region of a radial inflow turbine at off-design operating condition. They investigated that the tangential velocities of the fluid exiting along the pressure surface were higher compared to those along the suction surface. The degree of swirl near the tip was high and radial velocities were low throughout the cross-section except pressure surface tip corner region which was caused due to the interaction of the tip clearance flow with the main flow.

Sellgren, A. et al[3] [1999] have observed experimentally that in case of industrial suspension the pump head and efficiency reduces in the best efficiency region. The efficiency is more affected by this suspension than head. The rheological properties of slurries above were determined from differential pressure drop. With the inclusion of suspensions, pressure drop increase slowly with the flow rate as compared to the linear increase with a Newtonian medium. Pumping highly viscous Newtonian fluids means very large drops in efficiency and a shift of BEP to smaller flow rates, i.e., a larger pump has to be chosen. However, operation with a highly non-Newtonian suspension at lower flow rates shows an unstable head curve. It was investigated that with the scrubber sludge there was sharp reduction in head at flow rates below 40% of the BEP-value.

Majidi, K. et al[4] [2000] have observed the secondary flow in volute and circular casings of centrifugal pumps. The static pressure was not distributed uniformly at the outlet of the impeller which results in the radial thrust. The maximum relative velocity occurred at the

periphery of the impeller. The analysis shows that the curvature of the casings creates pressure gradients that cause vortices at cross-sectional planes of the casings.

Ogut, A. et al[5] [2000] have provided an insight into the effectiveness of fluid injection as a boundary layer control method in suppressing or eliminating flow separation in the vaned diffuser at off-design flow conditions. The reverse flow was observed along the hub and shroud walls. They also reduced the phenomenon of flow separation along the walls by injecting the fluid. The pressure recovery will be maximum if injection rate was 3% to the 60% of design flow rate.

Medvitz, R. B. et al[6] [2001] have used a multi-phase CFD method to analyze centrifugal pump performance under developed cavitating conditions. The differential model employed was the homogeneous two-phase Reynolds-Averaged-Navier-Stokes equations, wherein mixture momentum and volume continuity equations were solved along with vapor volume fraction continuity. The head coefficient at low cavitation numbers decreases rapidly for all flow coefficients. Local flow field solution plots shows clearly the principal physical mechanisms associated with the onset of cavitation breakdown. Results were also presented which illustrate the full three dimensional views of cavitating blades at the inlet.

Gandhi, B. K. et al[7] [2001] have compared the performance of two centrifugal slurry pumps for three solid materials having different particle size distribution (PSD) in terms of head, capacity, and power characteristics. The results have shown that the values of head and efficiency ratios were not only dependent on solid concentration but were also affected by PSD of the solids and properties of the slurry. The addition of fine particles in the slurry of coarser material leads to reduction in the additional losses that occur in the pumps due to the presence of solids. With the increase in the pump size, the additional losses due to presence of solids reduce.

Engin, T. et al[8] [2001] have conducted the experimental study on the effects of solids in an unshrouded centrifugal pump impeller by varying the tip clearance when both handling water and solid-water mixtures. The tip clearance loss mechanisms seem to be

similar to those in single phase pumping and a steady deterioration in pump performance was observed by increasing the tip clearances. The tip leakage losses increase as the tip clearance increases. The head reduction factor (*RH*) appears to be almost independent of the variation in the tip clearance, and which allows correlating the solids effects on the pump performance regardless of changes in the tip clearance. A slight decreasing trend was also observed in efficiency ratio when the tip clearance was increased.

Miner, S. M.[9] [2001] has worked on FLOTRAN to obtain solutions for the flow field and pressure field within the impeller of a mixed flow pump. Results produced include circumferentially averaged velocity and pressure profiles at the leading and trailing edges of the impeller. At the hub both the axial and tangential velocities were lower than the velocities at shroud and at the trailing edge the axial velocity profile shows the opposite trend from the leading edge, with the peak velocity shifted down toward the hub. Both the circumferentially averaged data and the blade passage results provide sufficient detail to evaluate the performance of the impeller.

Kouidri, S. et al[10] [2002] has studied the extraction of rubble carried out by means of a hydraulic circuit composed of a set of special pumps for slurry and of a horizontal hydraulic pipe. The optimal control of the whole installation requires continuous assessment of the mass flow rate of the solid–liquid mixture. It was aimed to develop a methodology of mass flow rate measurement to replace the existing limited method of gamma-densitometer, as the irregularities noticed during various phase measurement reduce the reliability of this technique.

Baun, D. O. et al[11] [2003] have observed the comparison between the characteristics of the lateral impeller forces and the hydraulic performances of four and five vane impeller operating in the spiral volute, concentric volute and double volute. The hydraulic performances of the two impeller designs were compared in each of the three different volute configurations. The force characteristic for the four vane impeller was similar to the five vane impeller in each respective volute casing. The best efficiency point shifts to a lower flow rate and the relatively rapid droop in the head and efficiency characteristics of the double volute at high flows was likely to be the result of increased volute losses.

The losses in the double volute will increase over the single volute because of more wetted surface and two tongues, which result in twice the incidence losses as compared to the single volute.

Zhou, W. et al[12] [2003] have used a CFD code to study three-dimensional turbulent flow through water-pump impellers during design and off-design conditions. Three different types of centrifugal pumps were considered in this simulation. One pump had four straight blades and the other two had six twisted blades. It was found that pumps having six twisted blades were better than those for pumps with straight blades, which suggests that the efficiency of pumps with twisted blades will also be higher than that of pumps with straight blades. It was also found that when the flow rate decreased below a certain value of the design flow rate, backflow occurred near the pressure surface of the pump impeller.

Kato, C. et al[13] [2003] have observed boundary interface between impeller and volute casing by using overset grids from dual frames of reference. The overall grid was composed of several grid sets, and appropriate transactions take place at the interface regions. Large-eddy simulation was applied to the prediction of internal flows in a high–specific-speed, mixed-flow pump stage that possesses weak instability in its head-flow characteristics at low flow-rate ratios. The head-flow characteristics were also developed, although the LES predicted the stall point at a somewhat lower flow-rate ratio than did the measurements. The phase-averaged distributions of the meridional- and tangential-velocity components were also compared with those measured by an LDV.

Nursen, E. C. et al[14] [2003] have developed an incompressible flow solver for the pump volute. The flow inside the volute of a centrifugal pump was three dimensional and, depending upon the position of the inlet relative to the cross-section center line, a single or double swirling flow occurs. The developed flow solver provides detailed pressure and velocity distribution information inside the volute, and the calculated results were verified by means of the experimental results. Calculations were performed at three different mass flows, one of which corresponds to the design's point mass flow. The calculated volute flow conditions namely, the variation in static pressure and total

pressure and the through flow and swirling component of the flow velocity over the cross-sections, which were located at various circumferential positions.

Kochevsky, A. N. et al[15] [2004] presents a review of simulation and computation technology for fluid flows in centrifugal hydromachines using modern CFD software tools and describes the capabilities implemented in these tools. They showed that the CFD tools used were adequate for modeling of complex physical phenomena occurring in fluid flows in hydraulic machine components and computing these flows within appropriate duration. These tools provide the user with convenient interface for input of source data and analysis of solution results. These tools also provide powerful capabilities for precise prediction of performance characteristics of hydraulic machines at the design stage allowing for saving resources for carrying out physical experiments.

Hergt, P. et al[16] [2004] have observed the unsteady velocity, pressure and flow angle at the impeller outlet of a centrifugal pump with and without volute casing at five operating points using the hotwire technology and a fast response single hole cylindrical probe. The test fluid was air. While the velocities and pressures depend only on the axial coordinate and were rotationally symmetrical, if there was no casing around the impeller, the influence of the volute on the circumferential distribution of these quantities increases with the deviation of the operating point from the design point. With respect to the local through flow distribution, this influence was much more pronounced in comparison to the pressure distribution.

Xu, C. et al[17] [2005] have calculated the detailed flow structures in the volute and the compressor performance was calculated for different tongues. It was observed that the flow in the volute sections has a single vortex structure, as opposed to two counter-rotating vortices. The round tongue creates significant blockage near the tongue. This blockage forces secondary flow center away from the tongue area. It was shown that the round tongue produces better performance than the sharp tongue. The detailed flow simulation was observed to better understand the volute flow mechanisms and provide design guidance in volute design to meet performance goals. The detailed flow structures for different volute tongue geometries were studied in detail.

Bakir, F. et al[18] [2005] have observed the flow behaviour in side the impeller passage and at the intersection of the impeller and volute. The flow was relatively uniform for all the blade passages. The impeller-volute assembly requires the addition of two extended computational domains; one at the impeller inlet and the other at the volute outlet. The Frozen-Rotor interface model was considered for the study of the impeller-volute assembly. A procedure for designing the volute, the non structured grid generation in the volute, and the interface flow passage between the impeller and volute were also discussed.

Ogata, S. et al[19] [2006] have observed the effect of surfactant additives on centrifugal pump performance experimentally. The total pump head of surfactant solution increased and the shaft power of surfactant solution decreased, comparing to those of tap water. The pump efficiency with surfactant solutions was also increased in comparison to that with tap water. It was also observed that the maximum flow rate of the pump increased with the use of surfactant solutions. The pump efficiency of surfactant solutions increased with an increase in surfactant concentration.

Shujia, Z. et al[20] [2006] have done a virtual performance experiment of centrifugal pump. From the calculated simulation result, a detailed situation of the flow in the pump was visualized, including the pressure distributions and velocity distributions. The performance curve was also drawn from the simulation result. The results have been modified according to design theory of centrifugal pump. It was observed that the minimum static pressure area appears at the back of the blade at impeller inlet regions. The rising flow speed of the fluid from impeller inlet to outlet was maximum at the outlet of impeller. Moreover, valuable information to the pump's performance optimization can also be provided by analysis of computational results.

González, J. et al[21] [2006] have observed relationship between the global variables and the dynamic flow structure numerically obtained for a low specific speed centrifugal pump. A previously developed unsteady flow model was used to correlate the dynamic field with the flow characteristics inside the impeller and volute of a single-stage

commercial pump. The solution was obtained by using viscous incompressible Navier-Stokes equations to get a 3D unsteady flow model. A sliding mesh technique was applied to take into account the impeller-volute interaction. The pressure forces seem to be the main driven mechanism to establish the flow features both in the impeller and volute, for a wide range of operating conditions.

Anagnostopoulos, J. S.[22] [2006] has developed a numerical model for the numerical solution of the RANS equations in the impeller of a centrifugal pump, and it was applied for a direct flow analysis and for the prediction of the impeller characteristic operation curves. The increased velocities were observed at the inlet of the blade due to blockage of flow. The minimum pressure was observed at suction side at the inlet of the blade. The flow equations were discretized using the control volume approach, whereas the standard k-ε model was adopted for the turbulence closure.

Min-Guan, Y. et al[23] [2007] have observed the phenomena of two-phase flow with salt crystallizing in the chemical pump, the 3-D turbulent flow in the impeller of chemical pump was simulated at the condition of rinsing. The internal flow between the impellers of chemical pump was investigated. Based on the Reynolds-averaging N-S equations and the standard k-ε two equations turbulent model, the simulations of turbulent flow between the impellers were performed using the flow computing software Fluent under different operating conditions. Based on the analysis of the calculated results of velocity and pressure profiles in the chemical pump and experimentally observed phenomenon of flow impact, secondary flow and recirculation, some design improvements were proposed, which give suggestions on the optimal design and internal two-phase flow study of the chemical pump.

Iancu, F. et al[24] [2007] have done numerical analysis on the blade geometry generation techniques for centrifugal compressor and shown that the performance improvements can be attributed to better surface finish, more accurate geometric definition (tighter dimensional tolerances), well-defined edges, and the lack of blade tip fillet on shrouded impellers. It has been investigated through experimental investigations that the construction method of the impellers has an impact on performance. The blade with

straight line elements has more temperature and pressure rise as compared to the curved blades. Numerical results will help understand the causes of the performance differences as well as the effects of straight line element blades on the flow through the impeller.

Spence, R. et al[25] [2007] have observed that operation of centrifugal pumps can generate instabilities and pressure pulsations that may be detrimental to the integrity and performance of the pump. A range of parameters and three flow rates were investigated and the pulsations were extracted at fifteen different locations covering important pump regions. The transient flow results compared reasonably with experimental data obtained in a limited experimental survey and clearly indicated that the blade suction face at outlet experiencing the largest pulsation levels. It was also noted that monitoring pulsations at the top dead centre of the pump volute casing would provide a better indication of internal pump pulsations than monitoring at the discharge.

Feng, J. et al[26] [2007] have investigated the unsteady flow and the pressure fluctuation in radial diffuser pumps. Calculations were performed at different operating points, radial gaps, and blade number between the impeller and diffuser. Computational results show that a jet-wake flow structure was observed at the impeller outlet. The biggest pressure fluctuation on the blade was found to occur at the impeller trailing edge, on the pressure side near the impeller trailing edge, and at the diffuser vane leading edge. All the flow rates, blade number configuration, and radial gaps influence significantly the pressure fluctuation and associated unsteady effects in the diffuser pumps.

Hofmann, M. et al[27] [2007] have done both experimental and numerical work on 3D cavitating flows. To observe experimental results a high speed video with the light sheet illumination were used. Numerical calculation was based on the 3D code, to predict the cavitation behaviour in turbo-machinery. This model was applied to the centrifugal pump geometry. Non-cavitating and cavitating conditions were investigated. Calculations were found to be in good agreement with experimental measurements and visualizations. Three regions for the occurrence of cavitation were observed, first at the shroud – blade interface, second at the suction side of blade, and third were at the hub at the inlet of the blade.

Pullum, L. et al[28] [2007] have observed that centrifugal pumps were the workhorse of hydraulic conveying systems but their performance was derated when viscous non-Newtonian fluids, such as pastes or coarse solids were present. The reduced performance for purely viscous Newtonian fluids may be calculated and then compared. The pump's performance was unaffected by the lower viscosity material with the lower yield stress, whereas the high viscosity fluid has derated the pump's performance appreciably. This method predicts the dramatic characteristic reduction in head at low flow rates that was often observed and explains why larger pumps were relatively insensitive to this form of head deration. Head deration due to the presence of coarse particles in Non- Newtonian carrier fluids was seen to follow similar trends to that of Newtonian suspensions and often dominates the total deration procedure.

Younsi, M. et al[29] [2007] have observed the influence of design parameters on the unsteady flow in a centrifugal fan using numerical and experimental investigations. The study showed the effects related to irregular blade spacing, blades number, and radial distance between the impeller periphery and the volute tongue. The alteration in the blade spacing does not alter the aerodynamic characteristics of the fan. The smaller number of blades generates a non-homogenous flow field particularly at the impeller periphery. The numerical results have been compared with the experimental measurements and a correlation between the wall pressure fluctuations and the far field noise signals has been found.

Younsi, M. et al[30] [2007] have observed the splitter blades effect on the performance of a centrifugal pump through both numerical simulation and experimental results. The analysis shows that, by adding splitter blades to the impeller, the impeller periphery velocities and pressures become more homogeneous. The influence of splitter blades on the velocity and pressure fields in a centrifugal impeller has been analyzed by means of 3D simulations. The splitter blades increases the head rise compared to the original impeller because of the impeller slip factor which helps conduction of the flow. But the efficiency was not improved since the hydrodynamic losses were greater. It decreases the pressure fluctuations and reorganizes more conveniently the flow at the volute outlet. But

for all the studied flow rates it increases the interaction between the volute tongue and the flow. The consequence was an increase of the radial thrust.

Cheah, K. W. et al[31] [2007] have numerically calculated the centrifugal pump internal flow field by using numerical methods and compared with experimental data over the wide flow range. The numerical simulation has permitted to study the internal flow pattern and pressure distribution of the pump operating at design point and off-design point. At design point, the internal flow or velocity vector was very smooth along the curvature along the blades. However, flow separation developed at the leading edge due to non tangential inflow conditions. The pressure increases gradually along the stream wise direction. The pressure lines were seen to be inclined in the circumferential direction. It was also observed that the isobars were no longer perpendicular to the impeller suction surface at low flow rate.

Motivation of present work

Computational fluid dynamics (CFD) analysis is being increasingly applied in the design and simulation flow in centrifugal pumps. With the aid of the CFD approach, the complex internal flows in water pump impellers, which are not fully understood yet, can be well predicted, to speed up the pump design procedure. With the development of CFD theory and the study of related numerical calculation in practice, 3D numerical simulation of inner flow inside a centrifugal pump has become possible. However, compared to other turbo machine domains, such as spaceflights, aviations, steam turbine and water turbine, the study of centrifugal pumps is relatively less. Numerical simulation makes it possible to visualize the flow condition inside a centrifugal pump, and provides valuable information to centrifugal pump's hydraulic design. By using simulation result to calculate or predict the performance of a centrifugal pump, to replace or reduce the performance experiments in the process of pump design, a great deal of labor and facility will be saved, as well as its shortening design cycle. Therefore, great improvement on centrifugal pump design must be achieved by CFD analysis of inner flow inside a centrifugal pump and following application of its results in pump design processes.

The objective is to develop a generalized design code for the centrifugal pump and then by using CFD software numerically investigate the flow field inside the centrifugal pump impeller passage. It applies ANSYS-CFX, a kind of CFD software, to calculate inner flow field by simulation and thereby obtains the speed of inner flow field and pressure-distributing condition. Thereafter, the performance curves of the centrifugal pump, calculated by using simulation results, are developed.

CHAPTER 3

CENTRIFUGAL PUMPS AND ITS DESIGN

3.1 PUMP

A pump is a device used to move liquids from lower pressure to higher pressure, and overcomes this difference in pressure by adding energy to the system. Pumps work by using mechanical forces to push the material, either by physically lifting, or by the force of compression. Early applications of pumps include the use of the windmill or watermill to pump water. Today, the pump is used for irrigation, water supply, gasoline supply, air conditioning systems, refrigeration (usually called a compressor), chemical movement, sewage movement, flood control, marine services, etc. Because of the wide variety of applications, pumps have a plethora of shapes and sizes, from very large to very small, from handling gas to handling liquid, from high pressure to low pressure, and from high volume to low volume.

3.2 PUMP CLASSIFICATIONS

Pumps are in general classified (fig: 3.1) as Roto-dynamic pumps and Positive Displacement pumps.

3.2.1 Positive displacement pump

Positive-displacement pumps are another category of pumps. Types of positive-displacement pumps are reciprocating and rotary pumps. Positive-displacement pumps operate by forcing a fixed volume of fluid from the inlet pressure section of the pump into the discharge zone of the pump. These pumps generally tend to be larger than equal-capacity dynamic pumps. Positive-displacement pumps frequently are used in hydraulic systems at pressures ranging up to 5000 psi. They also provide a fixed displacement per revolution and, within mechanical limitations, infinite pressure to move fluids.

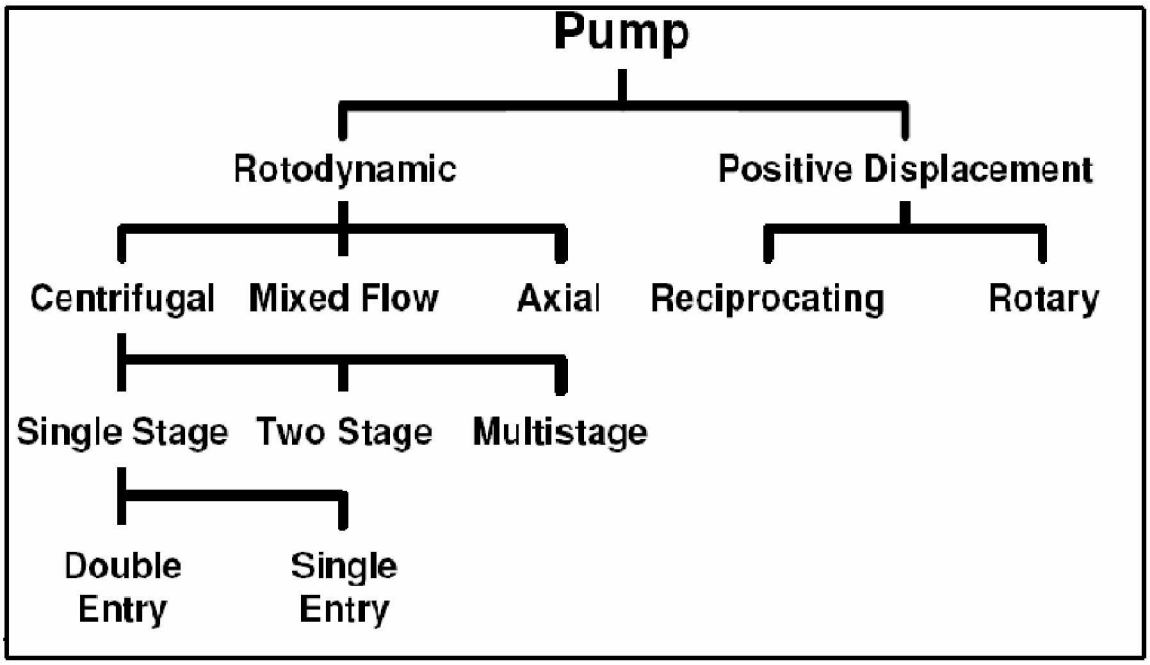

Fig 3.1 Classification of pump

A positive displacement pump will create whatever pressure is necessary to supply a constant amount of fluid for every stroke or revolution. Because these pumps always attempt to deliver a set quantity of fluid regardless of system pressure, a relief valve must be installed to protect both the pump and piping system from possible over-pressurization by the pump. Positive displacement pumps are self-priming meaning that they will create suction strong enough to draw fluid up into its suction side from a tank below.

a) Reciprocating pumps are one type of positive displacement pump. In a reciprocating pump, a volume of liquid is drawn into the cylinder through the suction valve on the intake stroke and is discharged under positive pressure through the outlet valves on the discharge stroke. The discharge from a reciprocating pump is pulsating and changes only when the speed of the pump is changed. This is because the intake is always a constant volume. Often an air chamber is connected on the discharge side of the pump to provide a more even flow by evening out the pressure surges. Reciprocating pumps are often used for sludge and slurry.

The reciprocating pump can be either single or double-acting. A single-acting design, shown in fig [3.2], discharges liquid only in one side of the piston or plunger. Only one

suction and one discharge stroke per revolution of the crankshaft can occur. The double-acting design takes suction and discharges on both sides of the piston resulting in two suctions and discharges per crankshaft revolution. Reciprocating pumps are generally very efficient and can develop high pressures. These pumps do however tend to be expensive.

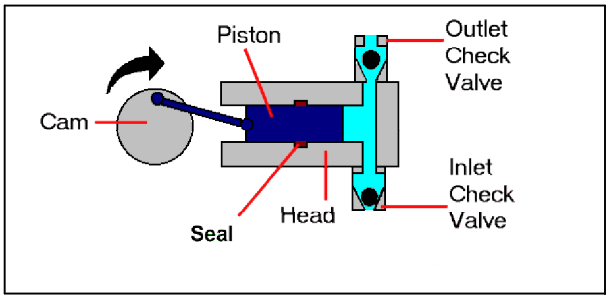

Fig 3.2 Cross sectional view of reciprocating pump

b) Rotary pumps work by means of rotating parts which trap liquid at the suction side and force it through the discharge outlet. The power end of a rotary pump is usually an electric motor or a turbine. Reverse rotation of a rotary pump will cause fluid flow backwards fig [3.3]. This situation could cause serious damage to a system by over-pressurizing the low pressure suction piping and by interrupting flow to the system.

They can handle almost any liquid that does not contain hard and abrasive solids, including viscous liquids. They are also simple in design and efficient in handling flow conditions that are usually considered to low for economic application of centrifuges. Types of rotary pumps include cam-and-piston, internal-gear, lobular, screw, and vane pumps. Gear pumps are found in home heating systems in which the burners are fired by oil. Rotary pumps find wide use for viscous liquids. When pumping highly viscous fluids, rotary pumps must be operated at reduced speeds because at higher speeds the liquid cannot flow into the casing fast enough to fill it. Unlike a centrifugal pump, the rotary design will deliver a capacity that is not greatly affected by pressure variations on either the suction or discharge ends. In services where large changes in pressure are anticipated, the rotary design should be considered.

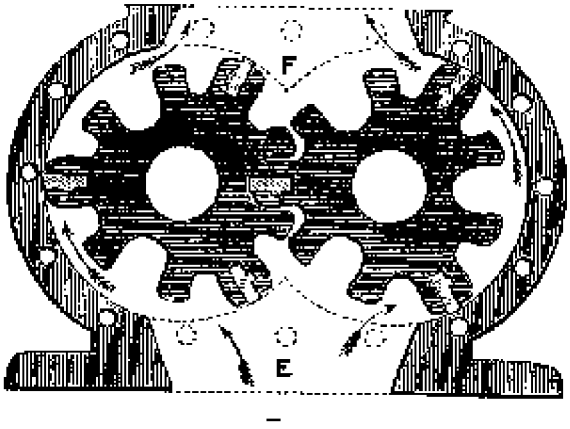

Fig 3.3 Cross sectional view of rotary pump

3.2.2 Rotodynamic pump

Rotodynamic pumps are one category of pumps under which there are several classes, two of which are: centrifugal and axial. These pumps operate by developing a high liquid velocity and converting the velocity to pressure in a diffusing flow passage. Rotodynamic pumps usually have lower efficiencies than positive displacement pumps, but also have lower maintenance requirements. Rotodynamic pumps are also able to operate at fairly high speeds and high fluid flow rates. These pumps are based on bladed impellers which rotate within the fluid to impart a tangential acceleration to the fluid and a consequent increase in the energy of the fluid. The purpose of the pump is to convert this energy into pressure energy of the fluid to be used in the associated piping system.

3.3 CENTRIFUGAL PUMPS

A centrifugal pump is a rotodynamic pump that uses a rotating impeller to increase the velocity of a fluid. Centrifugal pumps are commonly used to move liquids through a piping system. The fluid enters the pump impeller along or near to the rotating axis and is accelerated by the impeller, flowing radially outward into a diffuser or volute chamber, from where it exits into the downstream piping system. Centrifugal pumps are used for large discharge through smaller heads.

3.3.1 A BRIEF HISTORY

The centrifugal pump was developed in Europe in the late 1600's and was seen in the United States in the early 1800's. Its wide spread use, however, has occurred only in the last seventy-five years. Prior to that time, the vast majority of pumping applications involved positive displacement pumps. Since the 1940's, the centrifugal pump has become the pump of choice for many applications. Research and development has resulted in both improved performance and new materials of construction that have greatly expanded it's field of applicability. It is not uncommon today to find efficiencies of 93% for large pumps and better than 50% for small fractional horsepower units.

Most historians agree on the fact that Denis Papin (1647-1712) should be regarded as the originator of the centrifugal pump. Although the existence of centrifugal forces was probably known long before his time, and some machines were actually built which more or less made use of this force, he developed the first true centrifugal pump as we know it today: a machine in which water or air enters in axial direction near the shaft, is accelerated by revolving impeller blades and finally leaves the pump in circumferential direction. Earlier, the techniques which were used for raising water are the water wheel, the Archimedean screw, the chain of buckets, the Paternoster pump and the suction pump. Many of these devices were already in common use by the Ancients.

3.3.2 Working principle of centrifugal pump

A centrifugal pump works by the conversion of the rotational kinetic energy, typically from an electric motor or turbine, to an increased static fluid pressure. This action is described by Bernoulli's principle. The rotation of the pump impeller imparts kinetic energy to the fluid as it is drawn in from the impeller eye (centre) and is forced outward through the impeller vanes to the periphery. As the fluid exits the impeller, the fluid kinetic energy (velocity) is then converted to (static) pressure due to the change in area the fluid experiences in the volute section as shown in fig [3.4]. Typically the volute shape of the pump casing (increasing in volume), or the diffuser vanes, which serve to slow the fluid, converting to kinetic energy in to flow work, are responsible for the energy conversion. The energy conversion results in an increased pressure on the downstream side of the pump, causing flow.

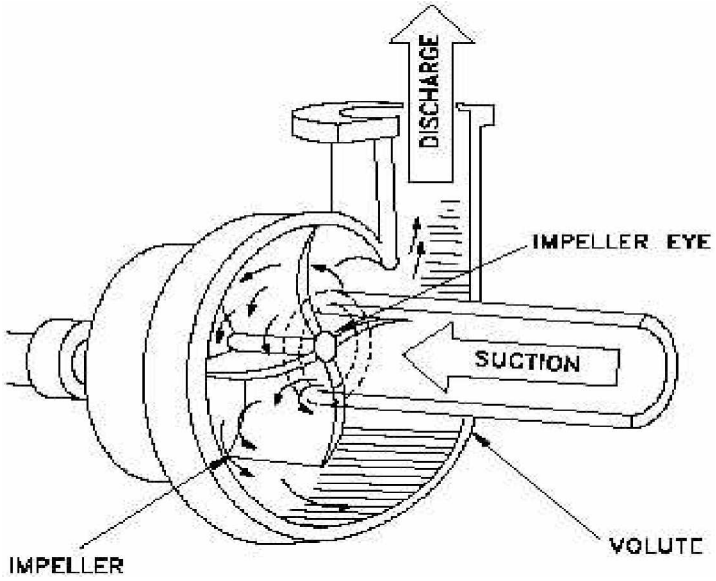

Fig 3.4 Working of centrifugal pump

3.3.3 Classification of centrifugal pumps: Centrifugal pump is classified as following way:

3.3.3.1 On the basis of the head:

- Low lift: Impeller is surrounded by volute & there are no guide vanes.
- Medium lift: They are generally provided with guide vanes.
- High lift: They are generally multistage pumps because single stage can not easily build up such a high pressure.

3.3.3.2 On the basis of the type of casing:

- Volute casing
- Diffusion pump
- Volute with vortex chamber

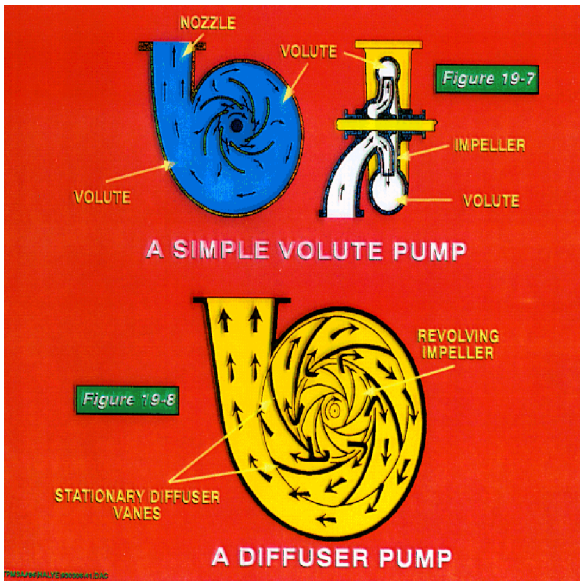

Fig 3.5 Volute casing and diffuser pump

3.3.3.3 On the basis of the number of stages:

Ø Single stage pump

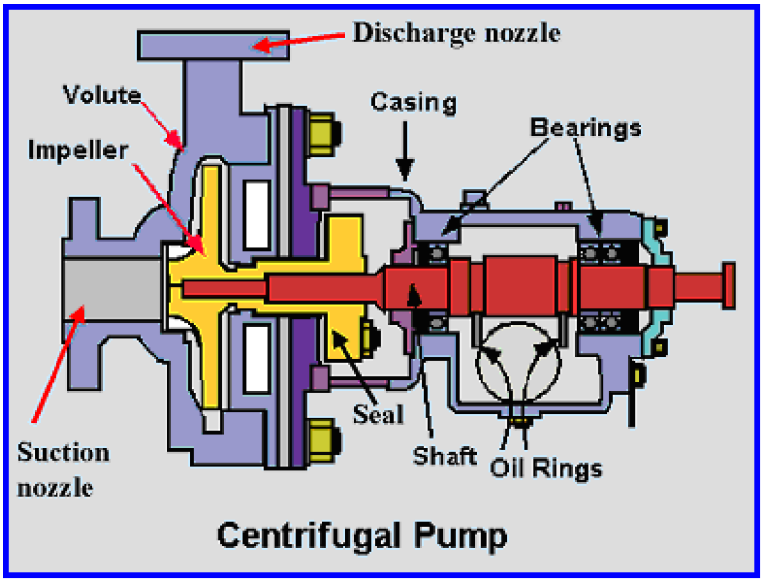

Fig 3.6 Single stage centrifugal pump

Ø Multistage pump

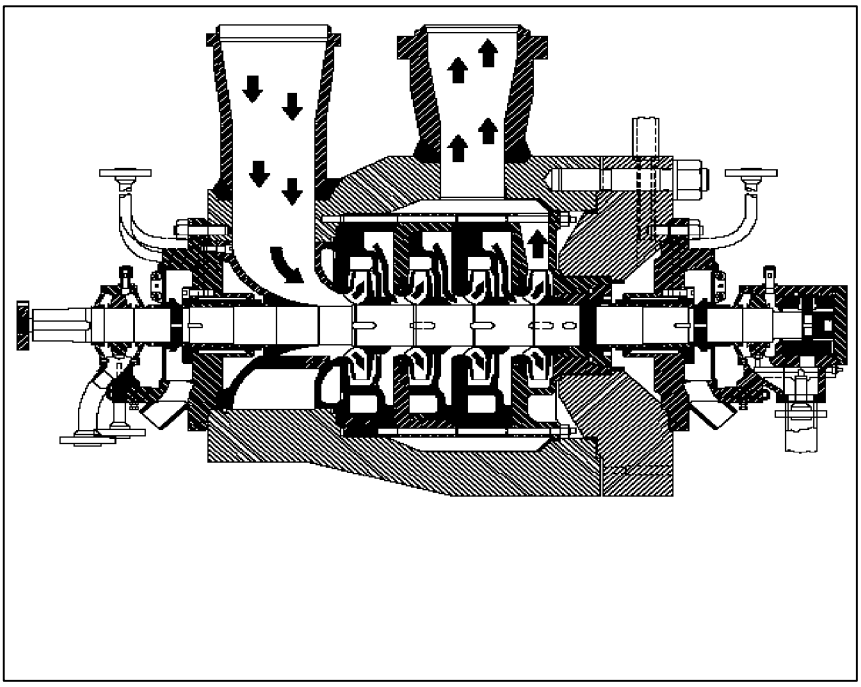

Fig 3.7 Multi stage pump

3.3.3.4 On the basis of the direction of flow through impeller:

- Ø Radial flow pump: Ordinarily all the Centrifugal pumps manufacture with radial flow impeller.
- Ø Mixed flow pump: Outlet mixed radial as well as axial combination. This is used for large quantity of water to low height.

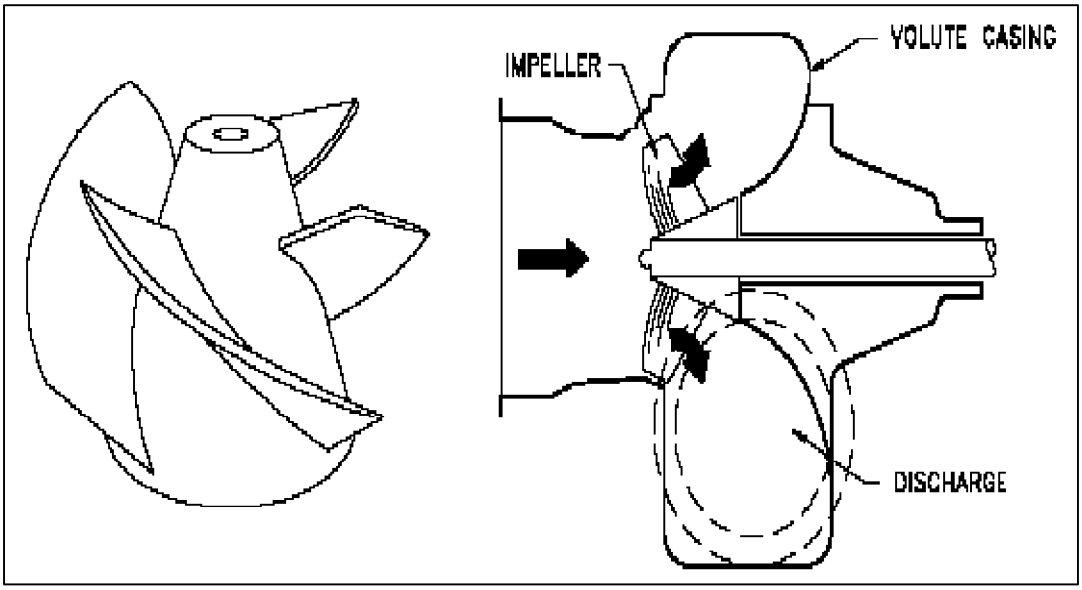

Fig 3.8 Mixed Flow pump

- Ø Axial flow pumps: Used in irrigation, high flow, low head.

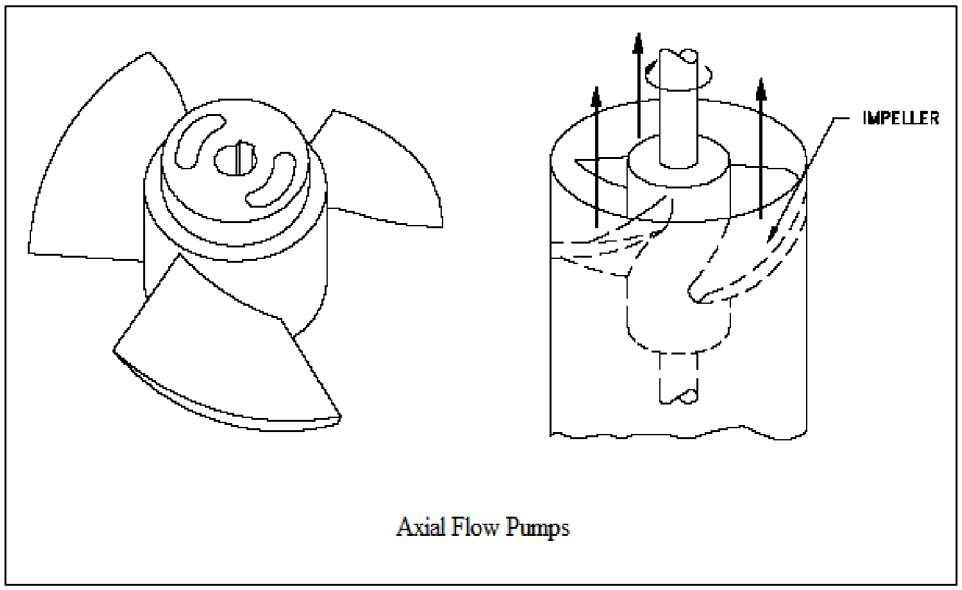

Fig 3.9 Axial flow pump

3.3.3.5 On the basis of the number of entrance to the impeller:

The pump may be single or double entry.

- Single entry or single suction pump: Water is admitted from a suction pipe on the side of impeller.
- Double suction pump: Admit water from both sides.

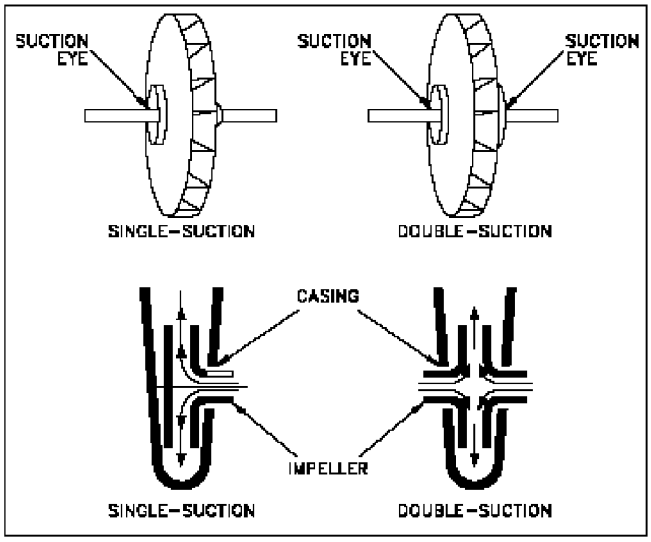

Fig 3.10 Single suction and double suction centrifugal pump

3.3.3.6 On the basis of the liquid handled:

Depending on the tube & viscosity of the liquid to be pumped, it may have

- Closed impeller
- Open impeller
- Semi open impeller

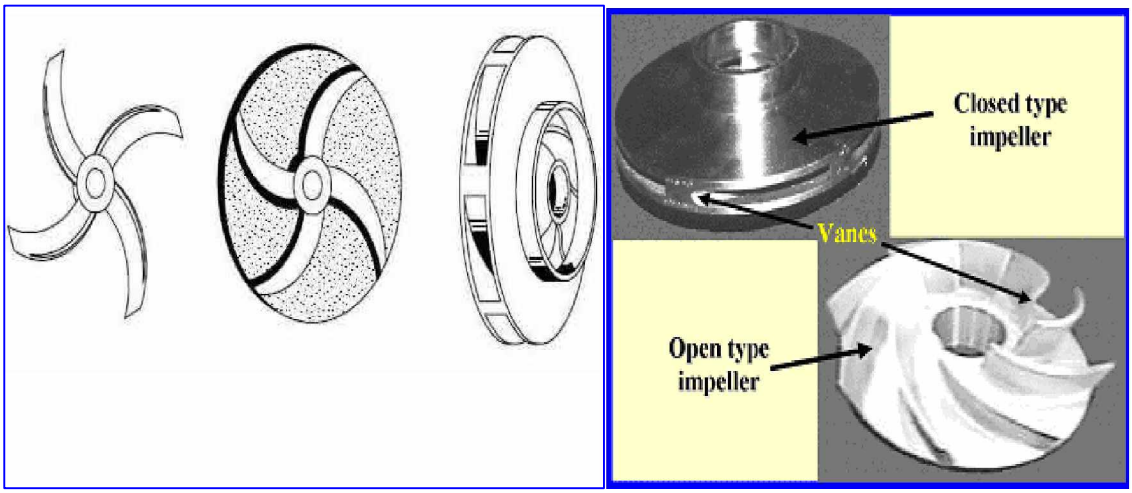

Fig 3.11 Closed, open and semi open impeller

3.3.3.7 On the basis of the specific speed:

- Slow speed radial flow runner- 10 to 30
- Normal speed radial flow impeller- 30 to 50
- High speed radial flow impeller- 50 to 80
- Mixed flow runner- 80 to 160
- Axial flow runner- 110 to 150
-

3.3.3.8 On the basis of the position of impeller:

- Horizontal impeller shaft pump
- Vertical impeller shaft pump

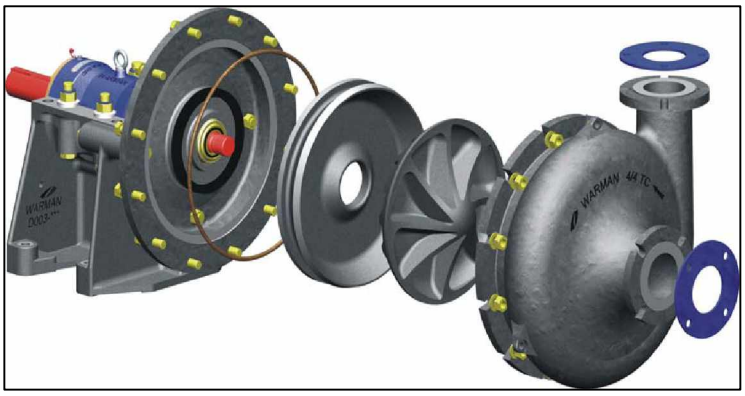

Fig 3.12 horizontal centrifugal pump

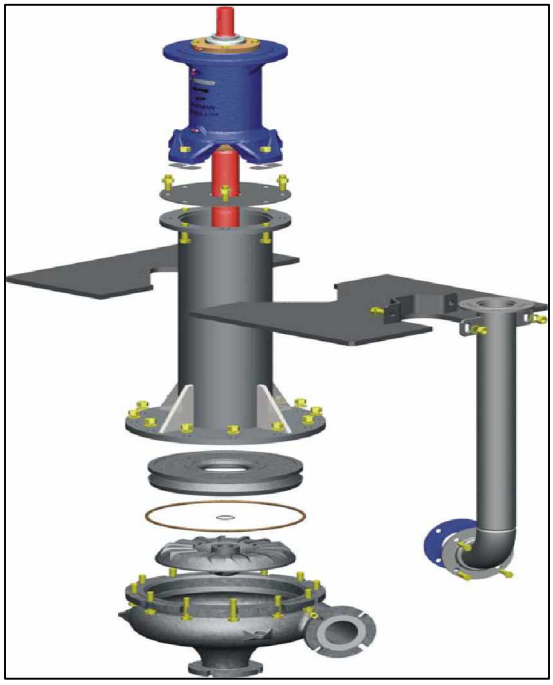

Fig 3.13 Vertical centrifugal pump

3.3.4 Centrifugal pump applications:

Pumps are used wherever any quantity of liquid must be moved from one place to another. Pumps are found in such services as steam power plants; water supply plants; sewage; drainage or irrigation; oil refineries, chemical plants & steel mills; food processing factories & mines; dredging or jetting operations; hydraulic power services & almost every ship whether driven by diesel or steam engine. While these pumps have much in common, they are varied to meet special requirements & particular needs of each service.

- Petroleum Industry
- Chemical Industry
- Paper Industry
- Water Supply
- Sewage & Sump Services
- Irrigation, Drainage & Flood Control
- Mining & Construction

3.4 CONVENTIONAL DESIGN OF PUMP:

Conventional design method of centrifugal pump are largely based on the application of empirical and semi-empirical rules along with the use of available information in the form of different types of charts and graphs in the existing literature. The design developed is best suitable for low specific speed centrifugal pump. Same design is also suitable for the design of high specific speed and multistage centrifugal pump with few modifications.

As the design of centrifugal pump involve a large number of interdependent variables, several other alternative designs are possible for same duty. Hence theoretical investigation supported by accurate experimental studies of the flow through the pump. Impeller as it is the element which transfers energy to the fluid stream influences the performance of the pump. Different authors have suggested different design procedure, method of calculation. The one which is used for this work is of Vasandhani[34.]

The problem of calculation of the dimension of an impeller and hence of the whole pump for given total head may have several solutions but they are not likely to be of equal merit, when considered from the point of view of efficiency and production cost. Designs suggested by Stepnoff, Lazarkiewicz, Kovats, Nyiri, Tuzson have been carefully studied. Each design parameter has been calculated using above procedures and an appropriate value adapt for present carefully analyzing the calculated values.

3.4.1 Input data

Initially, to start designing the impeller of the pump some parameters are assumed. Here Head (H), Flow rate (Q) and Pump speed (N) are assumed equal to 14.5 m, 0.016 m^3/sec and 1450 rpm respectively.

3.4.2 Design of impeller

3.4.2.1. Specific speed

Specific speed of the pump is computed based on the basis of head, flow rate and pump speed, different authors expressed the design parameter as function of specific speed. Specific speed is the important parameter in the design of the impeller because it gives information that which impeller should be used for that specific speed[34]. Generally, for the radial impeller specific speed varies from 10-40 and for mixed flow impeller it varies from 40-80.

$$N_s = \frac{N\sqrt{Q}}{H^{0.75}} \quad (3.1)$$

N_s = 24.683 rpm

The relationship between hydraulic and overall efficiency[34] is shown bellow which is used to find the hydraulic efficiency. $(1-\eta_h) = 0.66(1-\eta_o)$ (3.2)

Hydraulic Efficiency, η_h = 0.6436

And the overall efficiency is assumed to be 0.092 as per the recommendations of stepnoff's

Overall Efficiency, $\eta_o = \eta_h \times \eta_v \times \eta_m$ (3.3)

By using the equation for the overall efficiency the value of the mechanical efficiency can be calculated. Mechanical Efficiency, η_m =0.7768

3.4.2.2. **Input power and shaft power**: Having decided about the overall efficiency of pump, power to derive the pump ie. electric motor output, is found from the usual formula,

$$\text{Input power, } P_{in} = \left(\frac{\rho g Q H}{745\ \eta_0}\right) \quad (3.4)$$

Where,

g= Acceleration due to gravity

ρ=Density of the fluid

Input power required 15% more because of bearing and transmission losses. The suitable electric motor is then selected.

Calculated input power, $P_{in} = \frac{1000x9.81x0.016x14.5}{745x0.46} = 6.641$ HP

Shaft power, $P_{sh} = 1.15\ P_{in}$

Shaft Power, $P_{sh} = 1.15 \times 6.641 = 7.6373$ HP

3.4.2.3. Shaft diameter (d_{sh})

Since the speed of the pump has been already selected, hence for the shaft torque,

$$T = \left(\frac{P_{sh} \times 60 \times 750}{2\pi N}\right) \text{ N m} \quad (3.5)$$

Putting the values of P_{sh} and N in the above equation we get

T = 37472.5 N m

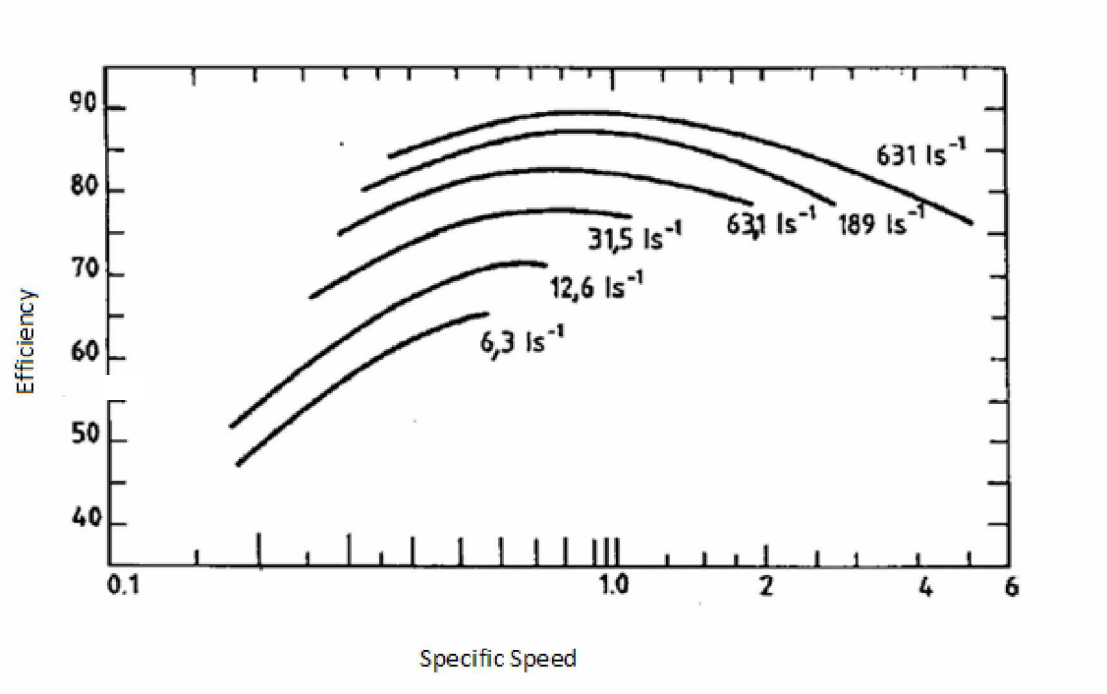

Fig 3.14 Variation of efficiency with specific speed[34]

Shaft Diameter can be calculated from the equation below

$$d_{sh} = \left(\frac{16T}{\pi F_s}\right)^{\frac{1}{3}} = 0.019689 \text{ m} \quad (3.6)$$

Where, F_s = 25 MPa, Stress depending on the material constant. For the present problem the shaft is assumed to be made of steel with an allowable shear stress of 25 MPa

3.4.2.4 Hub diameter (D_{hb}): The diameter of the hub is given as:

For given data D_{hb} = 1.2 x 0.019689 = 0.023627 m

3.4.3 Design of suction passage

1) Total discharge through the impeller

$$Q' = Q + \Delta Q \quad (3.7)$$

Where

Q = Flow rate at inlet

Q' = Flow rate at outlet

ΔQ = Flow rate losses or leakage losses

Q' = 0.016+0.016*0.08

Q' = 0.01728 m3/sec

2) Calculation of Axial Velocity at eye of impeller

The value of the axial velocity at impeller eye is found as shown below. For the given specific speed, assume the values of dimensionless parameters

$$C_A = 0.152\left(\frac{\sigma^2 \tan^2 \beta_3}{\tau^2 K}\right)^{\frac{1}{3}} \left(N^2 Q'\right)^{\frac{1}{3}} \quad (3.8)$$

C_A = 2.5469 m/s

Where,

C_A = Axial Velocity at entry of impeller.

Thoma cavitation factor, σ = 1.1 (Varies from 0.9 – 1.1)[34]

Circulation losses, τ = 1.05 (Varies from1.05 – 1.1)[34]

Constant, K = 0.84 (Varies from 0.75 – 0.85)[34]

Relative inlet angle at hub, $\beta_3 = 17.5$

3) Calculation of Eye Diameter (D_e):

The size of the passage on the basis of the equation of continuity, can be determined as,

$$Q' = \frac{\pi}{4}\left(D_e^2 K C_A\right)$$

But Q' is already been found, thus by using above equation value of eye diameter can be found.

$$D_e = \sqrt{\frac{4Q'}{\pi K C_A}} \qquad (3.9)$$

D_e =0.1014 m

D_e is the required diameter of the eye. The diameter at the blade inlet D_1, for low specific speed pumps will be slightly greater than D_e but with increase of specific speed, the inlet edge shifts towards suction and ultimately its value may be little less than D_e

$D_1 = 0.95 * D_e = 0.09633$ m

Generally there is slight contraction in the passage of an impeller while moving towards inlet of the blade from the impeller eye, thus the axial velocity at the eye is given as:

$C_0 = 1.05 * C_A = 2.6742$ m/s

$C_1 = 1.1 * C_0 = 2.9416$ m/s

Where,

C_1 = Absolute Velocity at inlet of the blade.

C_0 = Absolute Velocity at eye of the blade.

D_1 = Diameter at the inlet of the blade.

4) Breadth of the blade at the inlet (b_1): The values of D_1 and C_1 are calculated thus the breadth of the blade at inlet can be found as

$$b_1 = \frac{Q'}{\pi D_1 C_1} = 0.02135 \text{ m} \qquad (3.10)$$

5) Blade velocity at inlet (u_1)

$$u_1 = \frac{\pi D_1 N}{60} = 7.3135 \text{ m/s} \quad (3.11)$$

6) Blade inlet angle (β_1)

$$\beta_1 = \tan^{-1}\left(\frac{C_1}{u_1}\right) = 21.91°$$

3.4.4 Design of discharge passage

The governing equation for solution to outlet end dimensions is the Euler's equation. For rotation free inlet this may be written as

$$H_r = \frac{u_2^2}{g} - \frac{u_2 C_{2m}}{g}\cot\beta_2 \quad (3.12)$$

Where,

H_r = Total head generated

C_{1m} = Meridional flow velocity inside impeller

g = Acceleration due to gravity

u_1 = Blade velocity at outlet

The left hand side of this equation is related to total head generated as given below.

$$H_r = (1+p)\frac{H}{\eta_h} \quad (3.13)$$

= (1+0.32)* 14.5/0.6436

= 29.7389 m

Where,

η_h = 0.6436

p = 0.32 (Varies from 0.28 to 0.35)[34]

p is Pfleiderer's coefficient, a factor relating the difference between the imaginary and ideal conditions

The value of meridional flow velocity inside an impeller does not vary much and can be kept constant. However its value is generally somewhat lower than that at the suction end and so assume

$$C_{2m} = 0.9 * C_{1m} \quad (3.14)$$

$$= 0.9 * 2.9416$$

$$= 2.6474 \text{ m/sec}$$

Where,

C_{1m} = Meridional Flow Velocity at suction end.

β_2 (Outlet Blade Angle) is assumed to be as 26° (varies from 20°-26°)[34]

Substituting these values in Euler's equation (3.12)

$$29.7389 = \frac{u_2^2}{9.81} - \frac{u_2 \times 2.6474}{9.81} \cot 26^0$$

Blade velocity at outlet

u_2 = 20.0085 m/sec

Outer Diameter of impeller

$$D_2 = \frac{u_2 \times 60}{\pi N} \quad (3.15)$$

D_2 = 0.2635 m

3.4.5 Number of blades (Z)

$$Z = 2\pi \frac{D_1 + D_2}{D_2 - D_1} \sin 22 \quad (3.16)$$

$$= 5.06 \approx 5$$

3.4.6 Width of blade at outlet (B_2)

$$B_2 = \frac{Q'}{\pi D_2 C_{2m}} = \quad 0.0078848 \text{ m}$$

3.4.7 NPSH required

$$\Delta H = \lambda_1 \frac{W_2^2}{2g} + \lambda_2 \frac{C_2^2}{2g} \quad (3.17)$$

Take, λ_1=0.3 and λ_2 =1.2

Where λ_1 is the losses in the impeller whose value is dependent on the machine performance[34], λ_2 is losses in suction pipe.

$$W_2 = \frac{C_2}{\sin \beta_2} \tag{3.18}$$

$$= 8.8930$$

After substituting, ΔH = 1.6466 m

The results of the analytical work have been summarized below in table [3.1]:

Table[3.1]: Analytical result of the design.

No.	Design Parameter	Values
1	Specific speed of the pump	24.683
2	Hydraulic efficiency of the pump	00.6436
3	Mechanical Efficiency of the pump	0.776
4	Shaft power of the pump	7.6373 HP
5	Torque transmitted by the shaft	37472.5 N-m
6	Diameter of the Shaft	0.019689 m
7	Axial velocity	2.5469 m/s
8	Eye diameter	0. 09633 m
9	Inlet blade diameter	0.0963058 m
10	Hub diameter	0.0236283 m
11	Width at inlet	0.021342 m
12	Inlet blade velocity	7.3115 m/s
13	Outlet blade velocity	20.0085 m/sec
14	Outlet diameter of blade	0.2635 m
15	Number of blades	5
16	Breadth at outlet of blade	0.0078848 m
17	NPSH	1.6466

CHAPTER 4

COMPUTATIONAL FLUID DYNAMICS

Over the last 25 years, Computational Fluid Dynamics (CFD) has been increasingly used for a wide variety of engineering applications. In the beginning, the use of these techniques was customary only in the aerospace and nuclear fields. Subsequently, the use has spread to a variety of products, physical situations, and manufacturing processes. Some examples of interesting applications of computational modeling are cooling of electronics systems, rotating and reciprocating machinery, furnaces and combustion chambers, vehicle and building aerodynamics, chemical vapor deposition, plasma processing, refining hearths for alloys, and grain drying.

In such applications, computational modeling allows us to perform simulations of complex problems, investigate the effect of different design parameters, obtain detailed distributions of all relevant variables, and gain insight into the underlying physical processes. By a proper use of modeling, one can cut down on time consuming and costly experiments and field measurements, avoid design by trial and error, obtain speedy results, and design better products and processes.

Today's computers and computational techniques make it possible to include a very detailed representation of the problem and a comprehensive set of models for the relevant physical processes. However, it is often desirable to use some approximations and idealizations to reduce the computational expense. Then, computational modeling can be used in a routine manner in engineering design.

4.1 CFD PROCEDURE

In order to obtain better design in CFD, following procedure **(**Fig. 4.1**)** is applied so that fluid flow can easily be modeled in the centrifugal pump impeller.

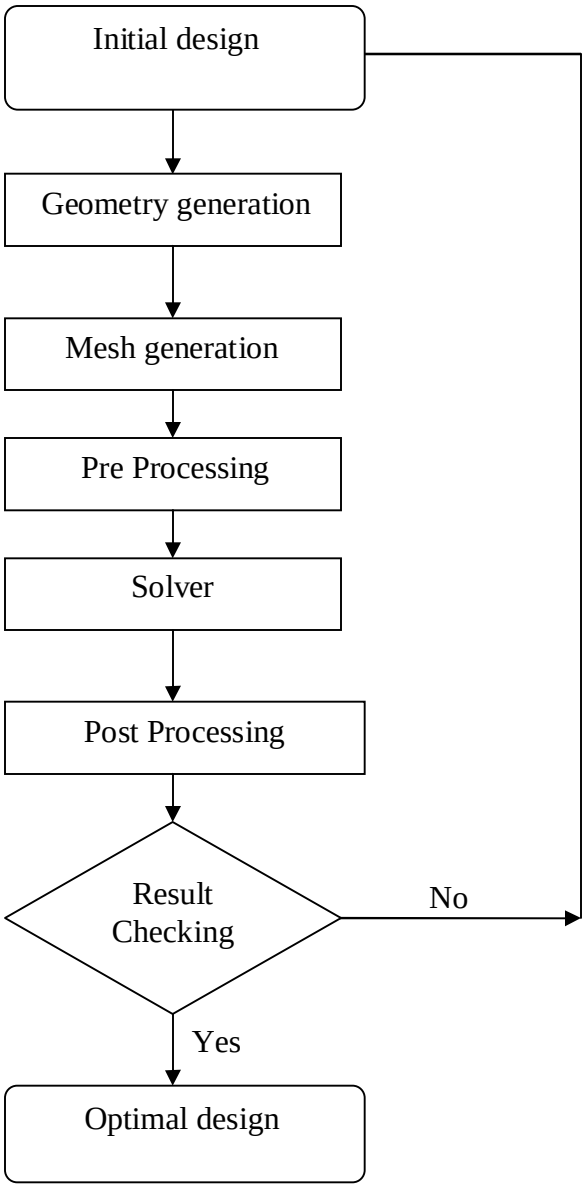

Fig 4.1: Flow chart of CFD procedure

4.1.1 Initial design and geometry generation

Initial design of the model is a planning decision and the geometry is generated depending on these initial design considerations, using either CFD modeling tools or other Design tools. This is the first stage for any design problem where all the pros and cons regarding the design of the problem are discussed. After completing the initial design the model is generated using different modeling software's.

Blade Modeler is a component of ANSYS-CFX[38]. The Blade Modeler software is a specialized, easy-to-use tool for the rapid 3-D design of rotating machinery components. Incorporating ANSYS, Inc's extensive turbomachinery expertise into a user-friendly graphical environment, the software can be used to design axial, mixed-flow and radial blade components in applications such as pumps, compressors, fans, blowers, turbines, expanders, turbochargers, inducers and others.

Blade Modeler provides the essential link between blade design and advanced simulation including computational fluid dynamics and stress analyses. Blade Modeler contains a rich set of tools and functions for designing a turbomachinery blade from scratch, using industry-specific tools, workflow, and language that the blade designer expects.

With Blade Gen, another component of ANSYS-CFX, the user can re-design existing blades to achieve new design goals or create completely new blade designs from scratch. When either re-designing or evaluating an existing blade design, Blade Gen facilitates the import of blade geometry interactively or through user supplied files.

4.1.2 Mesh generation

Mesh generation (Gridding) is the process of subdividing a region to be modeled into a set of small control volumes. Associated with each control volume there will be one or more values of the dependent flow variables (e.g., velocity, pressure, temperature, etc.) Usually these represent some type of locally averaged values. Numerical algorithms representing approximations to the conservation laws of mass, momentum and energy are then used to compute these variables in each control volume.

ANSYS TurboGrid[38] is a powerful tool that lets designers and analysts of rotating machinery create high-quality hexahedral meshes, while preserving the underlying geometry. These meshes are used in the ANSYS workflow to solve complex blade passage problems.

ANSYS TurboGrid employs the traditional concept of block-structure (multi-block) mesh generation. The block-structure approach is simple and efficient, allowing the well-known Transfinite Interpolation for surface and interior mesh generation to be used.

Although it is possible to establish a correspondence between any physical region and any given logically rectangular block, the grid inside such a block is likely to be unusable as the geometry becomes more complex. Topology blocks therefore represent contiguous sub-regions of a physical domain. Within each block, the mesh elements are logically rectangular but the blocks themselves fit together in an unstructured manner. Each block has its own curvilinear coordinate system and is logically rectangular. This allows the grid generation and numerical solution on the grid to be constructed to operate in a logically rectangular computational region. There are many subsets of Transfinite Interpolation, such as Lagrangian and Hermitic. There were many topologies which can be used in creating different topological blocks for the meshing of the blade geometry.

4.1.2.1 Topology

The topology is a structure of blocks that acts as a framework for positioning mesh elements. Topology blocks represent sections of the mesh that contain a regular pattern of hexahedral elements. They were laid out adjacent to each other without overlap or gaps, with shared edges and corners between adjacent blocks, such that the entire domain is filled. By using topology blocks to control the placement of hex elements, a valid hexahedral mesh can be generated to fill a domain of arbitrary shape. The topology is invariant from hub to shroud and is viewed or edited on 2-D layers which are located at various span wise locations.

The topology blocks can be arranged in a regular (structured) pattern, an irregular (unstructured) pattern, or in a pattern consisting of structured patches and unstructured patches. The choice of which approach should be followed should be based on whichever method minimizes the maximum skew of the topology blocks, since the skew in the hex elements of the mesh is directly related (differs only because of mesh smoothing). The topology should then be investigated at various layers (especially the hub and shroud layers) to check its quality since the mesh quality is directly dependent.

4.1.2.2 Different types of topologies used:

- H- Grid

H-Grid applies a topology of type H-Grid. An example of a topology of type H-Grid is shown in fig [4.2]**.**

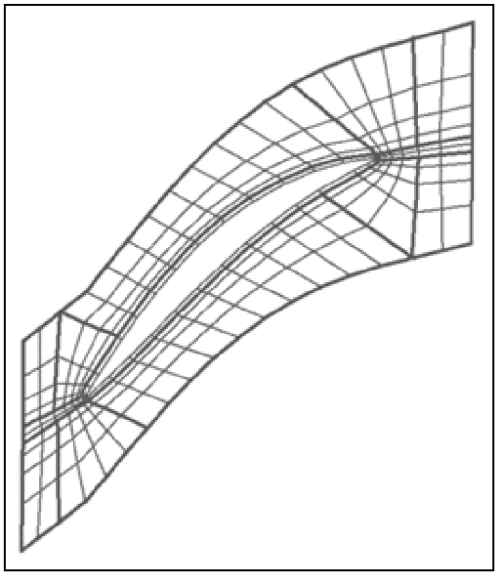

Fig 4.2 H- Grid topology

Ø J- Grid

J-Grid applies a topology of type J-Grid with an optional embedded O-Grid that surrounds the blade. An example of a topology of type J-Grid is shown in fig [4.3].

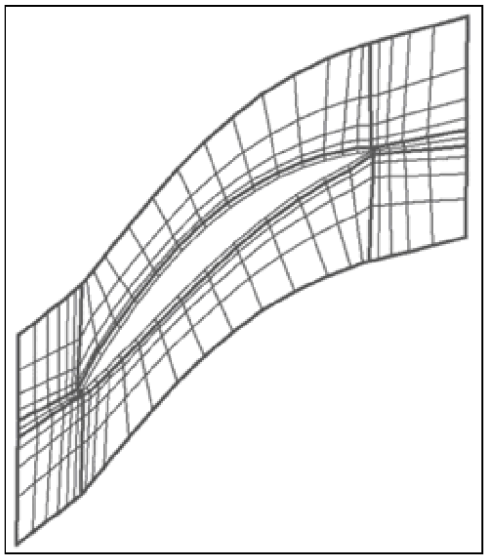

Fig 4.3 J-Grid topology

A topology of type J-Grid always wraps in opposite directions around the leading and trailing edges. An O-Grid is a topology that forms a continuous loop around the blade

profile (as would be seen in a blade-to-blade view). Using an O-Grid around the blade yields excellent boundary layer resolution and near-orthogonal elements on the blade.

- C- Grid

C-Grid is another available topology type for the leading and/or trailing edges when H/J/C/L Topology is selected. C-Grid topology is shown on the fig [4.4]**.**

- L- Grid

The L-Grid topology was used where upstream and/or downstream ends that did not have 1-to-1 periodicity. An example of a topology of type L-Grid is shown in fig [4.5]**.**

A key feature of ANSYS TurboGrid is the visibility of the surface mesh on the topology. As you adjust the topology, ANSYS TurboGrid adjusts the surface mesh in real time so that the true effect of topology changes is visible. To help identify problem areas in the surface mesh before you generate the full 3D mesh, you can visualize mesh statistics on the layers. Topology blocks generally contain the same number of mesh elements along each side. The mesh elements vary in size across topology blocks in a way that produces a smooth transition within and between blocks. This is accomplished by shifting the nodes toward, or away from, certain block edges. The topology blocks are positioned by default so that the mesh element sizes vary as smoothly as possible, given the constraints. When a suitable topology for the geometry was created meshing of the blade geometry was done.

The Ansys CFX can form meshes comprising one of the following element type shown in the fig [4.6]**.** The element type used here was hexahedral. These hexahedral elements have six faces and eight corners. Four types of meshes, coarse, medium, fine and user defined, are developed for the impeller passage, with number of nodes 20000, 100000, 300000 and 50000 respectively. Finer meshes are used to reduce the errors which occur due to approximation in the calculation. But, when the results of different meshes are

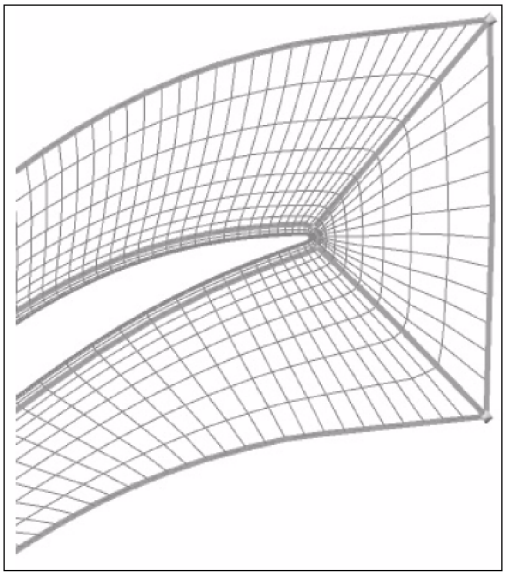

Fig 4.4 C-Grid topology

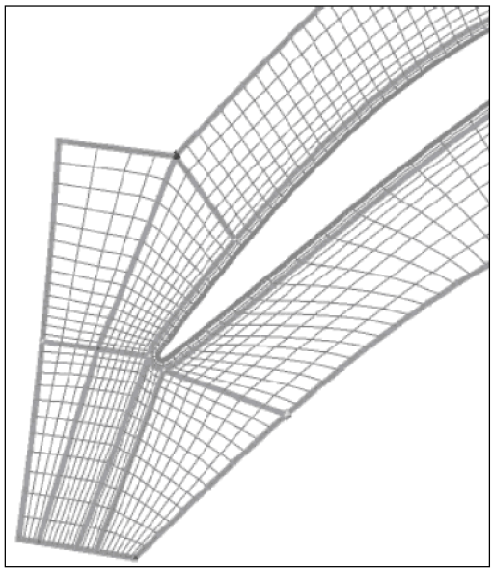

Fig 4.5 L-Grid topology

compared it is found that there is not much of difference in results. So to reduce the time of computation and amount of space required to solve the problem coarse mesh is used. The fig [4.6] depicts the impeller passage with coarse mesh.

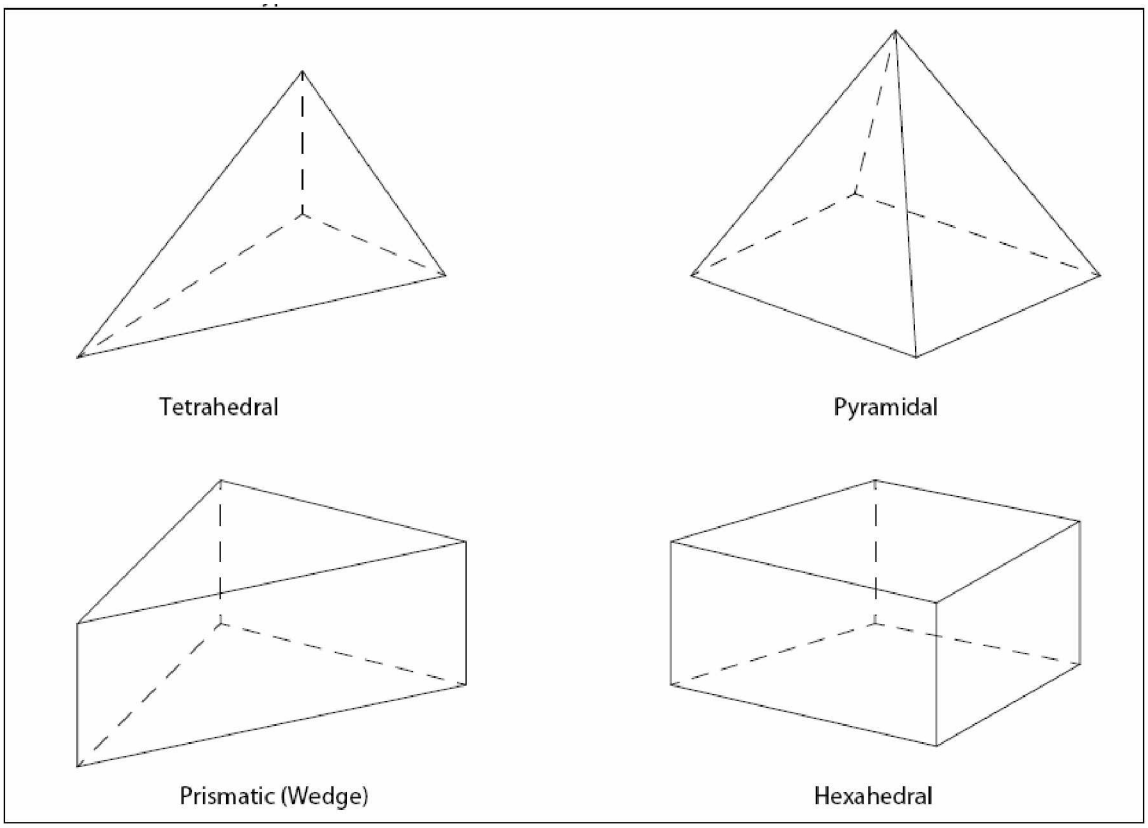

Fig 4.6 Different types of elements for grid generation

4.1.3 Pre-Processing

The operation preprocessing provides the solver with all necessary information for the calculation. The fig [4.7] shows a practical approach an overview of all decisions and definitions which are essential in this phase. In the first step called structure idealization it must be selected, whether it is an internal (e.g. crankcase of a motor with cooling channels) or external flow (e.g. windmill rotor). In the case of an internal flow the inlet and outlet openings have to be closed by so called lids. These parts must be added to the existing assembly and boundary conditions should be defined at their inner surfaces. The external flow volume, also called Computational Domain, is used for grid generation and influences both the result quality and the computing time.

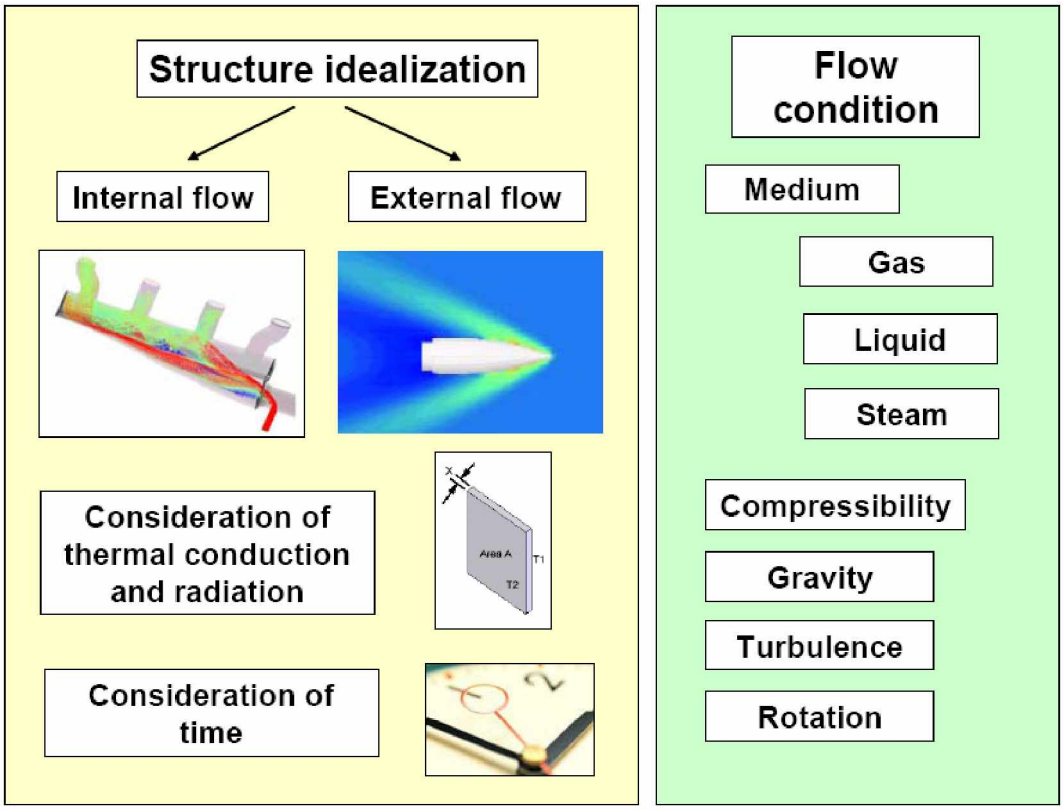

Fig 4.7 Introduction of Pre-Processing in CFD simulations

Typical flow systems have a complex geometry; furthermore the fluid also influences the whole system in different ways. For example forces and moments are generated within the structure as a result of deflections and the fluid pressure. The fluid temperature also causes a higher material temperature and as a consequence thermal deformations of the concerned parts. If it is necessary to consider the heat transfer in solids, radiation and the dependency of time, the according parameters have to be defined. Similar to all simulators the quality of results is very much depending on the accuracy of the material parameters. Concerning the fluid type liquids, gases and steam have to be distinguished. Of special interest is the Newtonian viscosity and the possible consideration of compressible fluids. The correct determination of boundary conditions provides the integration of the simulation model into the environment. Pressure and velocity define a given flow condition at the open components in the case of an internal flow. Thermal conditions can be applied to faces of given temperature or heat generation.

4.1.3.1 Boundary conditions

Setting up a flow-simulating computation involves specifying boundary conditions, a task needing careful thought. Fig [4.8] shows the definition block for boundary conditions. In particular, it involves the specification of convective and diffusive fluxes at surfaces bounding the domain. In Cartesian and cylindrical-polar coordinates, the location of boundary features (inlets, outlets, blockages, etc) can now be linked to named 'objects' defined during the grid-generation procedure. This obviates the need to enter the coordinates twice: once when defining the grid, and again when specifying boundary conditions.

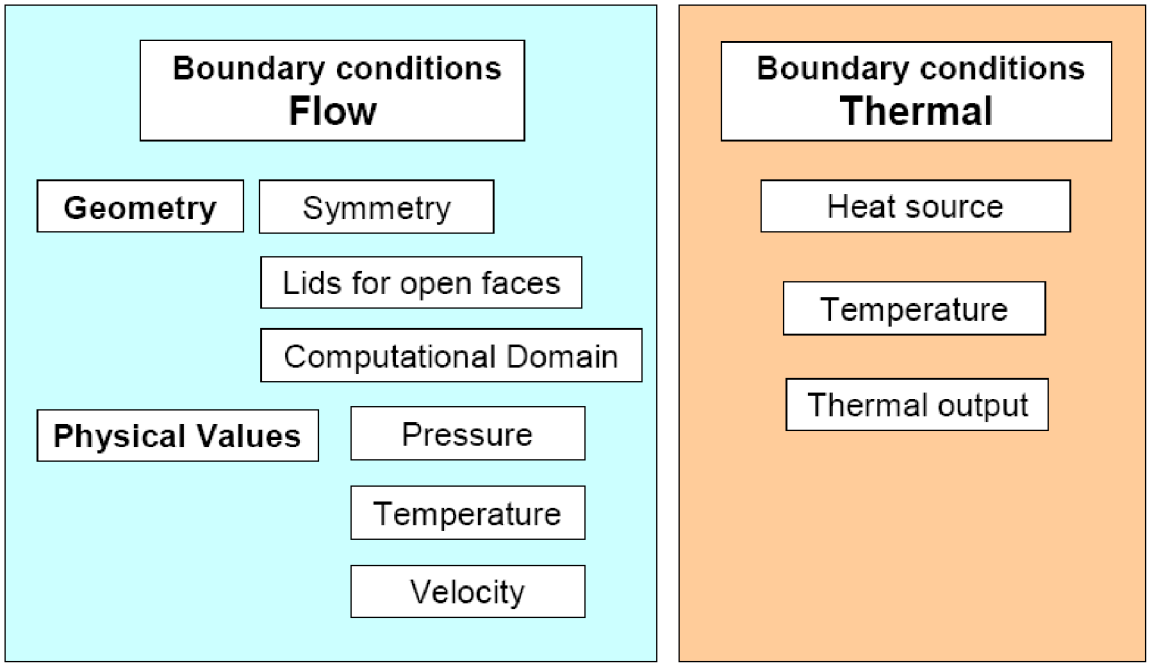

Fig 4.8 Introduction of boundary conditions

If an 'object' is subsequently repositioned or re-sized, then the boundary condition is also changed automatically. If an object is deleted, any associated boundary-conditions will also be deleted without further instructions from the user. If a new 'object' is created by copying an existing one, the boundary conditions are not automatically copied, but a new boundary condition may be linked to the new object. Similarly, heat sources can be attached to existing 'block-' or 'plate-type' boundary conditions, without re-entering their location. In compressible flows, when the flow speed at the outflow boundary is supersonic, it makes little difference how the boundary conditions are specified since

flow disturbances can't propagate upstream. In low speed and incompressible flows, however, disturbances introduced at an outflow boundary can have an affect on the entire computational region.

As a general rule, a physically meaningful boundary condition, such as a specified pressure condition, should be used at out flow boundaries whenever possible. When a continuative condition must be used it should be placed as far from the main flow region as is practical so that any adverse influence on the main flow will be minimal.
Generally, a pressure condition cannot be used at a boundary where velocities are also specified, because velocities are influenced by pressure gradients. The only exception is when pressures are necessary to specify the fluid properties, e.g., density crossing a boundary through an equation of state.The inlet condition for velocity and temperature can be specified using profile of grid. The turbulent kinetic energy k and its dissipations rate can be calculated from the value of turbulence intensity specified in the inlet.

4.1.3.2 Turbulence models

Turbulence consists of fluctuations in the flow field in time and space. It is a complex process, mainly because it is three dimensional, unsteady and consists of many scales. It can have a significant effect on the characteristics of the flow. Turbulence occurs when the inertia forces in the fluid become significant compared to viscous forces, and is characterized by a high Reynolds Number. In principle, the Navier-Stokes equations describe both laminar and turbulent flows without the need for additional information. However, turbulent flows at realistic Reynolds numbers span a large range of turbulent length and time scales, and would generally involve length scales much smaller than the smallest finite volume mesh, which can be practically used in a numerical analysis. The Direct Numerical Simulation (DNS) of these flows would require computing power which is many orders of magnitude higher than available in the foreseeable future.

Turbulence models are used to predict the effects of turbulence in fluid flow without resolving all scales of the smallest turbulent fluctuations. A number of models have been developed that can be used to approximate turbulence based on the Reynolds Averaged Navier-Stokes (RANS) equations. Some have very specific applications, while others can

be applied to a wider class of flows with a reasonable degree of confidence. One of the main problems in turbulence modeling is the accurate prediction of flow separation from a smooth surface. Standard two-equation turbulence models often fail to predict the onset and the amount of flow separation under adverse pressure gradient conditions. This is an important phenomenon in many technical applications, particularly for airplane aerodynamics since the stall characteristics of a plane are controlled by the flow separation from the wing. For this reason, the aerodynamic community has developed a number of advanced turbulence models for this application. In general, turbulence models based on the two-equations predict the onset of separation too late and under-predict the amount of separation later on. This is problematic, as this behavior gives an overly optimistic performance characteristic for an airfoil. The prediction is therefore not on the conservative side from an engineering stand-point. The models developed to solve this problem have shown a significantly more accurate prediction of separation in a number of test cases and in industrial applications. Separation prediction is important in many technical applications both for internal and external flows

a. The k-epsilon model

One of the most prominent turbulence models, the $k-\varepsilon$ (*k*-epsilon) model, has been implemented in most general purpose CFD codes and is considered the industry standard model. It has proven to be stable and numerically robust and has a well established regime of predictive capability. For general purpose simulations, the model offers a good compromise in terms of accuracy and robustness.

Within ANSYS CFX, the $k-\varepsilon$ turbulence model uses the scalable wall-function approach to improve robustness and accuracy when the near-wall mesh is very fine. The scalable wall functions allow solution on arbitrarily fine near wall grids, which is a significant improvement over standard wall functions. While standard two-equation models, such as the model, provide good predictions for many flows of engineering interest k is the turbulence kinetic energy and is defined as the variance of the fluctuations in velocity. It has dimensions of (L^2T^{-2}) m^2/s^2.ε is the turbulence eddy dissipation (the rate at which the velocity fluctuations dissipate), and has dimensions of

per unit time (L^2T^{-3}). The k- model introduces two new variables into the system of equations. The continuity equation is then:

$$\frac{\partial \rho}{\partial t} + \nabla \bullet (\rho U) = 0 \tag{4.1}$$

and the momentum equation becomes

$$\frac{\partial \rho U}{\partial t} + \nabla \bullet (\rho U \otimes U) - \nabla \bullet (\mu_{eff} \nabla U) = -\nabla p^{'} + \nabla \bullet (\mu_{eff} \nabla U)^T + B \tag{4.2}$$

where

B is the sum of body forces,

μ_{eff} is the effective viscosity accounting for turbulence,

$p^{'}$ the modified pressure.

b. The k-omega model

One of the advantages of the $k-\omega$ formulation is the near wall treatment for low-Reynolds number computations. The model does not involve the complex non-linear damping functions required for the $k-\omega$ model and is therefore more accurate and more robust The models assumes that the turbulence viscosity is linked to the turbulence kinetic energy and turbulent frequency via the relation:

$$\mu_t = \frac{k}{w} \tag{4.3}$$

μ_t = turbulence viscosity

k is the turbulence kinetic energy and is defined as the variance of the fluctuations in velocity w=turbulence frequency

c. The Shear Stress Transport (SST) model

The Shear-Stress-Transport model was designed to give highly accurate predictions of the onset and the amount of flow separation under adverse pressure gradients by the inclusion of transport effects into the formulation of the eddy-viscosity. This results in a major improvement in terms of flow separation predictions. The superior performance of this model has been demonstrated in a large number of validation studies (76) The SST model is recommended for high accuracy boundary layer simulations

$$v_t = \frac{a_{1k}}{\max(a_1\omega, SF_2} \tag{4.4}$$

Where

$$v_t = \mu_t / \rho$$

F_2 is a blending function

S is an invariant measure of the strain rate.

The SST is a Reynolds-averaged turbulence modeling approach that accounts for the turbulent stresses by representing only the mean quantities in a flow fields. SST combines the $k-\varepsilon$ and $k-\omega$ turbulence models via a blending function which forces $k-\omega$ in th boundary later and $k-\varepsilon$ in the freestream. Primarily, the SST model was developed to overcome deficiencies in the $k-\varepsilon$ and $k-\omega$ models. Therefore, using the SST model over these models is recommended.

4.1.3.3 Multiphase flow

Multiphase flow is a flow in which more than one fluid is present. In general, the fluids consist of different chemical species, e.g., air-water. In some applications, they may represent different thermodynamic phases of the same species, e.g., steam-water. It is important to distinguish between multi-component and multiphase flow. A multi-component fluid is assumed to consist of a mixture of chemical species which are mixed at the molecular level. In this case, single mean velocity and temperature fields, etc. are solved for the fluid. Examples are gaseous mixtures, and solutes in liquids. The fluids in a multiphase flow are assumed to be mixed at macroscopic length scales, much larger than molecular. Examples are gas bubbles in liquid, liquid droplets in a gas or in another immiscible liquid, etc. In this case, it is necessary to solve for different velocity and temperature fields, etc., for each fluid. These may interact with each other by means of interfacial forces and heat and mass transfer across the phase interfaces. For example, if cold wet particles are injected into a fast flowing stream of hot air, the particles will be accelerated by drag, they will be heated up by heat transfer across the phase boundary, and they will be dried by evaporation of water into water vapor at the phase boundary.

4.1.4 Solver

The different types of solvers which are used in computational fluid dynamics are

- Finite Difference Method
- Finite Volume Method (Control Volume Method)
- Finite Element Method

A finite difference method (FDM) discretization is based upon the differential form of the PDE to be solved. Each derivative is replaced with an approximate difference formula (that can generally be derived from a Taylor series expansion). The computational domain is usually divided into grids, and the solution will be obtained at each nodal point. The FDM is easiest to understand when the physical grid is Cartesian, but through the use of curvilinear transforms the method can be extended to domains that are not easily represented by brick-shaped elements. The discretization results in a system of equation of the variable at nodal points, and once a solution is found, then we have a discrete representation of the solution.

A finite volume method (FVM) discretization is based upon an integral form of the PDE to be solved (e.g. conservation of mass, momentum, or energy). The finite volume method comprise three main steps: First, the computational domain is divided into small control volumes (CV) in the mesh generating process. Each volume has a central point where properties such as temperature and velocity are calculated and a number of face areas.

For numerical reasons, it is common that some properties are calculated on the volume faces and some in the cell center. Second, the underlying equations are integrated over the CV. The sought parameters are momentarily considered to be known at the neighboring points and are approximated on the cell faces by means of interpolation. This approximation can be done by different numerical approaches, e.g. first and second order accurate. If desired, it is possible to use different interpolation schemes for each flow property. Since interpolation always depends on distance, the finite volume method is clearly grid dependent, and the mesh size should be as small as possible to increase

accuracy. To save computing time, it is advantageous if the grid can be made locally finer where large gradients are expected. In the third and last step, the control volumes are visited one at a time, an equation system is built and boundary conditions are included. The solution of the, commonly very large, equation system is always done in an iterative manner.

The basic advantage of this method over FDM is it does not require the use of structured grids, and the effort to convert the given mesh in to structured numerical grid internally is completely avoided. As with FDM, the resulting approximate solution is a discrete, but the variables are typically placed at cell centers rather than at nodal points. This is not always true, as there are also face-centered finite volume methods. In any case, the values of field variables at non-storage locations (e.g. vertices) are obtained using interpolation.

A finite element method (FEM) discretization is based upon a piecewise representation of the solution in terms of specified basis functions. The computational domain is divided up into smaller domains (finite elements) and the solution in each element is constructed from the basis functions. The actual equations that are solved are typically obtained by restating the conservation equation in weak form: the field variables are written in terms of the basis functions, the equation is multiplied by appropriate test functions, and then integrated over an element. Since the FEM solution is in terms of specific basis functions, a great deal more is known about the solution than for either FDM or FVM. This can be a double-edged sword, as the choice of basis functions is very important and boundary conditions may be more difficult to formulate. Again, a system of equations is obtained (usually for nodal values) that must be solved to obtain a solution.

Comparison of the three methods is difficult, primarily due to the many variations of all three methods. FVM and FDM provide discrete solutions, while FEM provides a continuous (up to a point) solution. FVM and FDM are generally considered easier to program than FEM, but opinions vary on this point. FVM are generally expected to provide better conservation properties, but opinions vary on this point also. If you are trying to decide which method to use, then the best path is probably found by consulting the literature in the specific problem area.

Flow equations

The steady, incompressible, Reynolds Averaged Navier-Stokes (RANS) equations are employed for the flow calculations in polar coordinates and a rotating with the impeller system of reference. These equations establish that changes in momentum in infinitesimal volumes of fluid are simply the sum of dissipative viscous forces (similar to friction), changes in pressure, gravity, and other forces acting inside the fluid: an application of Newton's second law.

They are one of the most useful sets of equations because they describe the physics of a large number of phenomena of academic and economic interest. They may be used to model weather, ocean currents, water flow in a pipe, flow around an airfoil (wing), and motion of stars inside a galaxy. As such, these equations in both full and simplified forms, are used in the design of aircraft and cars, the study of blood flow, the design of power stations, the analysis of the effects of pollution, etc. Coupled with Maxwell's equations they can be used to model and study magneto hydrodynamics.

The Navier-Stokes equations are differential equations which, unlike algebraic equations, do not explicitly establish a relation among the variables of interest (e.g. velocity and pressure). Rather, they establish relations among the rates of change. For example, the Navier-Stokes equations for simple case of an ideal fluid (inviscid) can state that acceleration (the rate of change of velocity) is proportional to the gradient (a type of multivariate derivative) of pressure.

Contrary to what is normally seen in solid mechanics, the Navier-Stokes equations dictate not position but rather velocity. A solution of the Navier-Stokes equations is called a velocity field or flow field, which is a description of the velocity of the fluid at a given point in space and time. Once the velocity field is solved for, other quantities of interest (such as flow rate, drag force, or the path a "particle" of fluid will take) may be found.

A two dimensional, laminar incompressible flow with constant viscosity is described by:

x-Momentum $$\rho \frac{\partial u}{\partial t} + \rho u \frac{\partial u}{\partial x} + \rho v \frac{\partial u}{\partial y} = \mu \left(\frac{\partial^2 u}{\partial x^2} + \frac{\partial^2 u}{\partial y^2} \right) - \frac{\partial \rho}{\partial x} \quad (4.5a)$$

y-Momentum $$\rho \frac{\partial v}{\partial t} + \rho u \frac{\partial v}{\partial x} + \rho v \frac{\partial v}{\partial y} = \mu\mu \left(\frac{\partial^2 v}{\partial x^2} + \frac{\partial^2 v}{\partial y^2} \right) - \frac{\partial \rho}{\partial x} \quad (4.5b)$$

and continuity $$\frac{\partial u}{\partial x} + \frac{\partial v}{\partial y} = 0 \quad (4.6)$$

There are several methods of discretizing a given differential equation, but finite volume method is used in ANSYS-CFX.

4.1.5 Post-Processing

Post-processing provides the CFD professional with easy-to-use powerful result visualization features for structured, unstructured, and hybrid grids. It provides an in depth view of data with visualization tools such as cutting planes, contouring, streamlines, line plots, data probes and animation. Animations can be created by saving CFD solutions with or without skipping certain number of time steps and playing the saved frames in a continuous sequence. Animations are important tools to study time-dependent developments of vertical /turbulent structures and their interactions.

CHAPTER 5

MODELING AND ANALYSIS

5.1 GEOMETRY GENRATION

Before the modeling of blade, a generalized program is written for the design of the blade. The program is based on the design methodology discussed in the previous chapter. The parameters which were considered initially are Head, Flow Rate, Pump Speed, Volumetric efficiency and Overall Efficiency. The output of the program is given in the Annexure II. Some of the output parameters of this design were used as input of the Blade Modeler.

The numerical model as shown in fig [5.1] was created using the Blade Modeler tool of ANSYS-CFX package. From the solid model of the impeller, a negative mold was created that describes the flow passages. This solid model was the base geometry for creating the finite volume mesh. Due to periodicity features of the impeller geometry, only one passage containing one main blade was modeled as shown in fig [5.2].

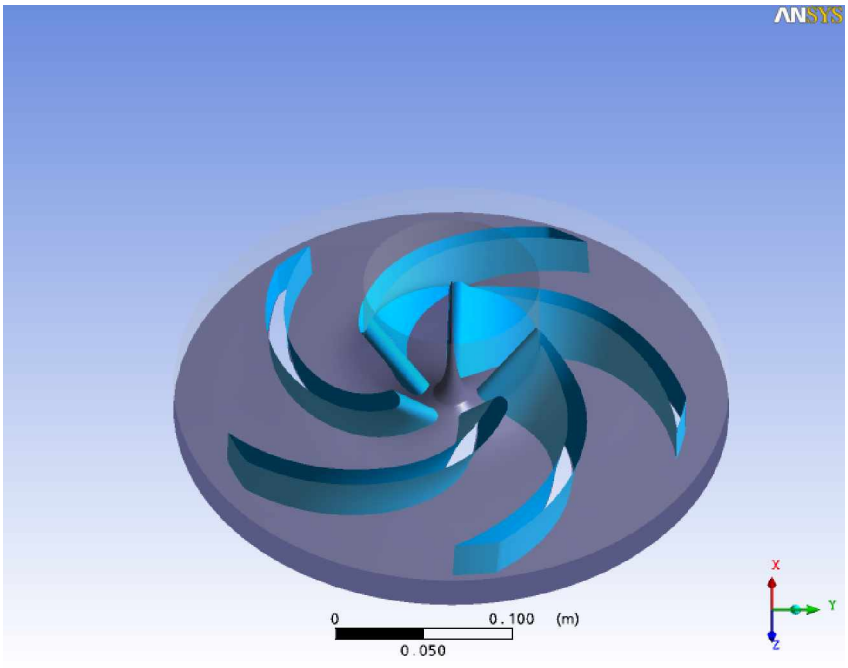

Fig 5.1 Solid model of impeller

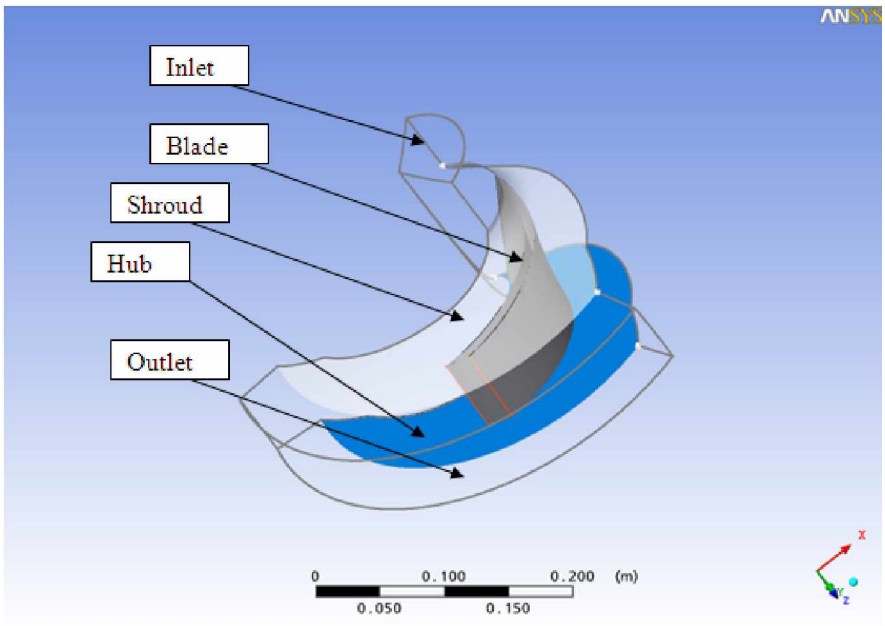

Fig 5.2 Impeller geometry of one blade

5.2 MESH GENERATION

The model of impeller which is used for the numerical investigation is created using Ansys-CFX Blade modeler. CFX – Turbogrid is used to generate grid around the blades of the impeller. Since the geometry of impeller is symmetric around the rotation axis, thus can be divided into number of passages which are all identical. For this investigation five passages are used and simulation is done on single passage. It is observed that with 3,00,000 nodes are required for adequate representation of viscous effects with shock waves and tip leakage, but also noted that useful results can be obtained with 1,00,000 nodes or lesser. Initially four different grids , fine having 3,18,897 nodes, medium having 1,28,079, coarse having 25,789 node and one having 65,136 nodes are used as shown below in fig[5.3]. Some effort has been made to focus on lesser grid sizes. The analyses were run for all the grid sizes at single flow condition with maximum residual convergence criteria being set to 10^{-04}.

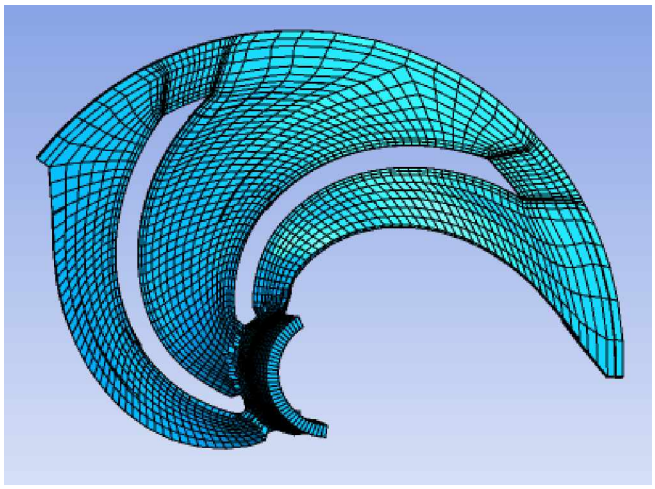

Fig 5.3(a) Model with coarse mesh

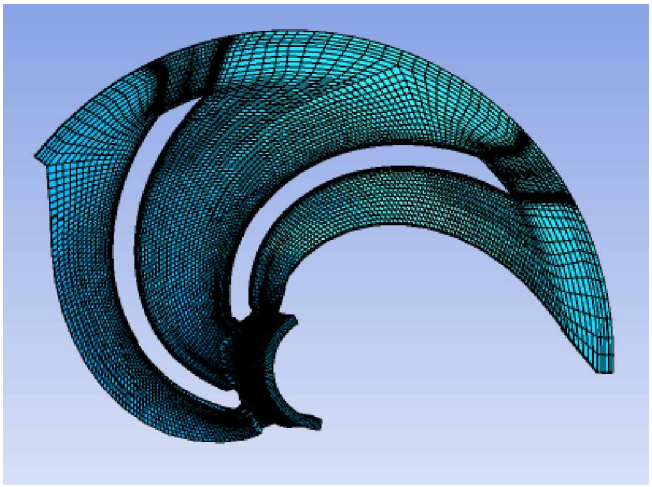

Fig 5.3(b) Model with medium mesh

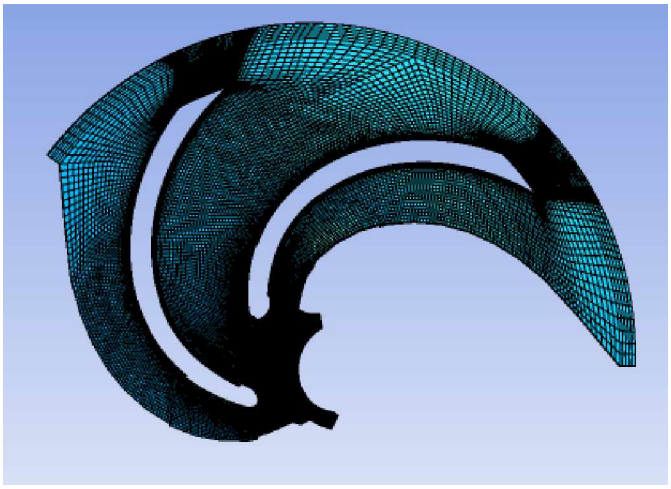

Fig 5.3(c) Model with fine mesh

The pressure distribution from inlet to the outlet is shown in fig [5.4]. This identifies that all grids predict the shape of the pressure variation consistently. This shows that there is not much variation in the solution for the grid with higher number of nodes. Thus coarse grid is used for other analyses done on this impeller passage. This choice of coarse grid is influenced significantly by the computing facilities available because these analyses take lots of time and memory. The Ansys CFX can form meshes comprising one of the element type shown in the fig [4.6]. The element type used for messing the impeller blade model is hexahedral. These hexahedral elements have six faces and eight corners. Four types of meshes, coarse, medium, fine and user defined, are developed for the impeller passage. Finer meshes are used to reduce the errors which occur due to approximation in the calculation. But, when the results of different meshes are compared it is found that there is not much of difference in results. So to reduce the time of computation and amount of space required to solve the problem coarse mesh is used. The fig [5.5] depicts the impeller passage with coarse mesh. The mesh generated in the Ansys Turbo Grid is imported in the Ansys-Pre. Thereafter the problem is physically modeled by defining the domain, source point, boundary conditions etc. The type of simulation for the given problem is steady state. After defining the primitives of the problem the boundary conditions are defined.

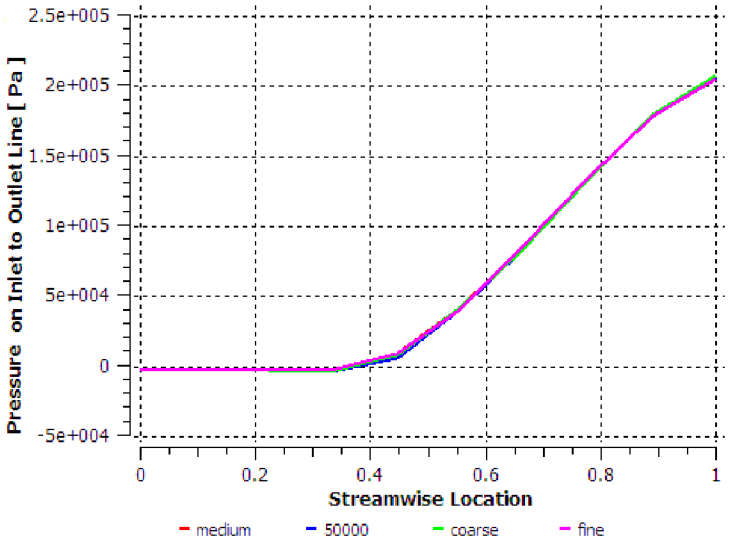

Fig 5.4 Pressure distribution in impeller along the streamline

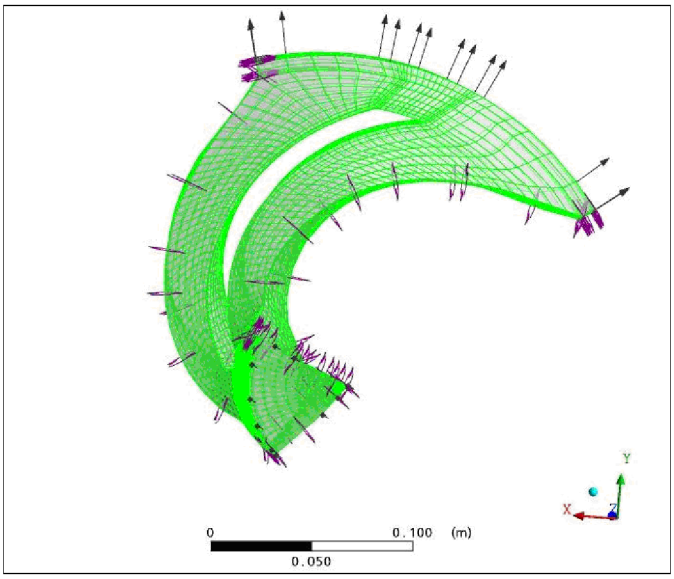

Fig 5.5 Impeller passage with coarse mesh

5.3 PRE-PROCESSING

The general parameters and boundary conditions used for 3D flow simulations of the impeller are summarized in the Table [5.1].

For all simulations the boundary conditions are as follows:

Table 5.1 Boundary conditions used for simulation.

PARAMETERS	BOUNDARY CONDITIONS
Flow simulation domain	Single impeller flow channel
Grid	Structured
Fluid	Water at standard conditions
Inlet	Pressure along rotation axis
Outlet	Imposed mass flow rate
Periodic	Two symmetry surfaces positioned in the middle of the blade passage
Wall	No Slip
Turbulence model	SST model
Discretization	Second order
Maximum residual convergence criteria	10^{-4}

After applying the boundary condition in the preprocessor the model is solved in the CFX-Solver. The errors in the solution disappear as the solver reaches the required convergence criteria within the given number of iterations. The solved model is then post processed to get the required results in the CFX-Post.

CHAPTER 6

RESULTS AND DISCUSSIONS

The outcome and their analysis is the main part of any research work. In the present work the outcome of the programmed code for the design of impeller is used for the modelling and thereafter, the numerical investigation is done on the impeller of the centrifugal pump.

6.1 OUTPUT OF IMPELLER DIMENSIONS

Input data

Head = 14.5 m, Flow rate = 0.016 m^3/sec, Speed = 1450 rpm

Table 6.1 Output of impeller dimensions

S. NO.	OUTPUT IMPELLER DIMENSIONS	VALUE
1	Specific speed of pump	24.6832
2	Hydraulic efficiency of pump	0.6436
3	Mechanical efficiency of the pump	0.77688
4	Input power of the pump	7.6373 HP
5	Input power of the pump in Watts	5689.8 W
6	Torque	37472.5 Nm
7	Diameter of shaft	0.01969 m
8	Axial velocity	2.5487 m/sec
9	Eye diameter	0.10137 m
10	Inlet blade diameter	0.096305 m
11	Hub diameter	0.02362 m
12	Width at inlet	0.021342 m
13	Inlet blade velocity	7.3115 m/sec
14	Inlet blade angle	21.9318°
15	Outlet blade velocity	20.5262 m/sec
16	Outlet blade diameter	0.27036 m
17	Number of blades	5
18	Width of blade at outlet	0.007678 m

19	NPSH required	1.64
20	Outlet blade angle	26°

6.2 NUMERICAL RESULTS

6.2.1 Flow distribution in impeller at different span

The pressure increases gradually along stream wise direction within impeller passage and has higher pressure in pressure side than suction side of the impeller blade. However, the pressure developed inside the impeller is not so uniform. The isobar lines are not all perpendicular to the pressure side of the blade inside the impeller passage; this indicated that there could be a flow separation because of the pressure gradient effect. The fig [6.1] shows the pressure distribution within the impeller at three different spans ie.20, 50 and 80.

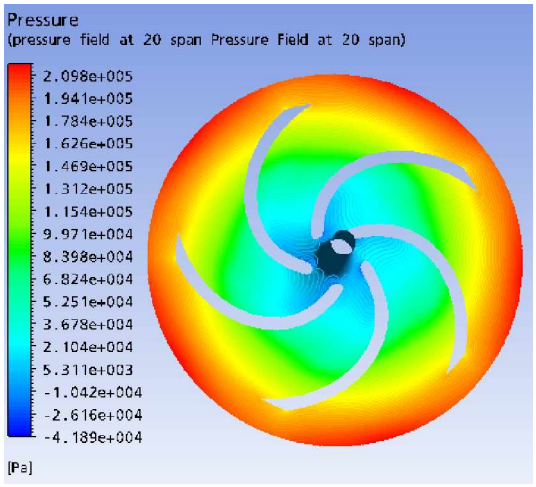

(a)

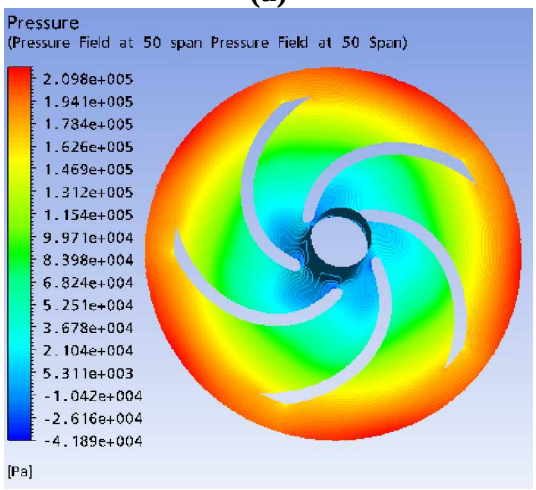

(b)

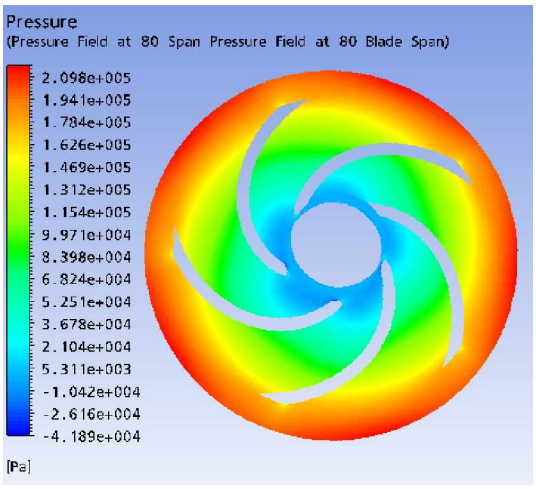

(c)

Fig 6.1 Pressure distribution at 20, 50, 80 span

Velocity also increases gradually along streamwise direction within the impeller passage. As the flow enters the impeller eye, it is diverted to the blade-to-blade passage. The flow at the entrance is not shockless because of the unsteady flow entering the impeller passage. The separation of flow can be seen at the blade leading edge. Since, the flow at the inlet of impeller is not tangential to the blade, the flow along the blade is not uniform and hence the separation of flow takes place along the surface of blade. Here it can be seen that flow separation is taking place on both side of the blade, ie, pressure and suction side as shown in fig [6.2].

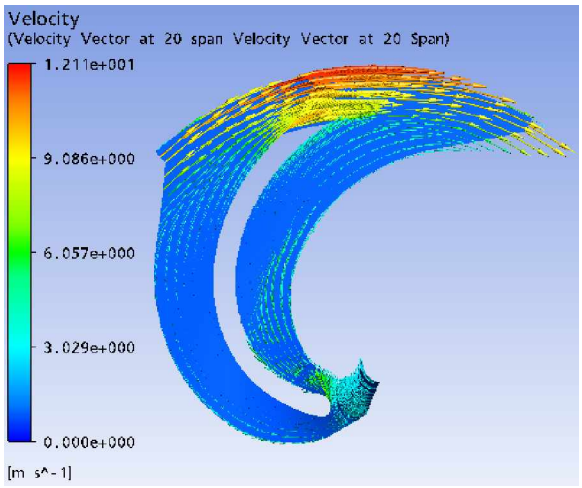

(a)

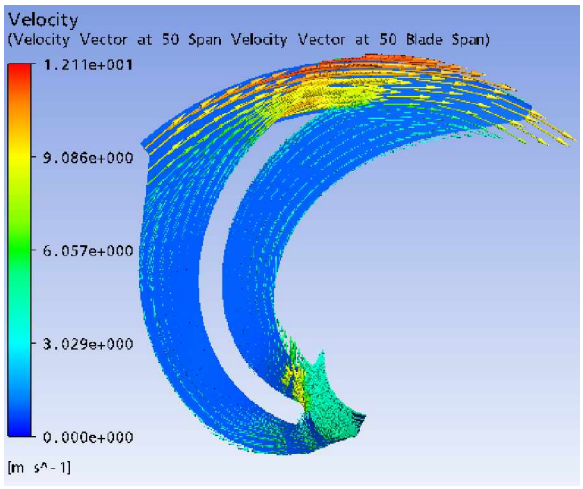

(b)

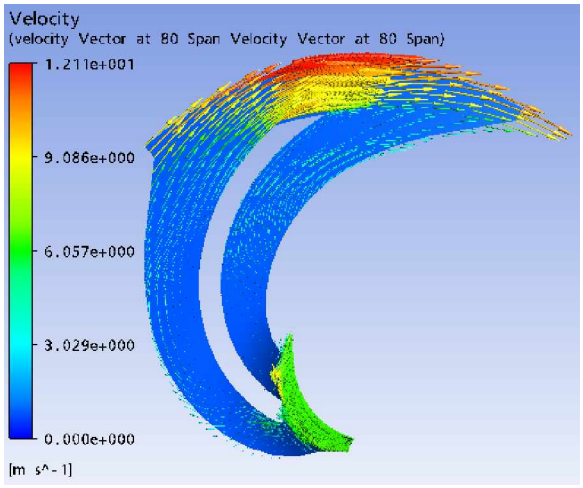

(c)

Fig 6.2 Velocity distribution at 20, 50 and 80 span

6.2.2 Pressure and velocity between impeller blades

The distribution of total pressure between the blades of the impeller is shown in the fig [6.3]. The lowest total pressure appears at the inlet of the impeller suction side. This is the position where cavitation often appears in the centrifugal pump. The highest total pressure occurs at the outlet of impeller, where the kinetic energy of flow reaches maximum. The fig [6.4] shows the static pressure distribution at the span of 50 between the blades of the impeller. It is observed that the static pressure inside the impeller blades is asymmetry distributed. The minimum static pressure area appears at the back of the impeller blade ie suction side, at the inlet. The fig [6.5] shows the relative velocity distribution at 50 span between two blades of the impeller. The rising flow speed of the

fluid from inlet to outlet reaches maximum at the impeller blade outlet. From the pressure distribution plot, pressure gradient changes gradually from inlet radius to outlet radius for each impeller. In order to transmit power to the liquid, pressure on the leading or pressure side of the vane should be higher than pressure on the suction side of the vane. Any force exerted by the vane on the liquid has an equal and opposing reaction from the liquid and this can exist only as a pressure difference on two sides of impeller vanes. The immediate effect of such a pressure distribution is that relative velocities near the suction side of the impeller vanes are higher than those near the pressure side of the vane as shown in the fig [6.6].

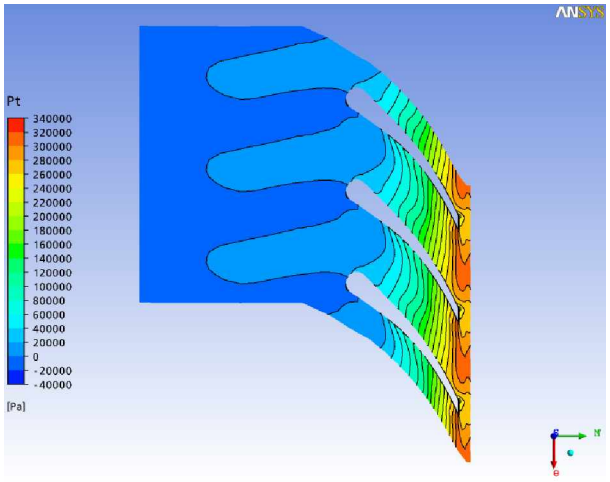

Fig 6.3 Distribution of total Pressure at 50 span

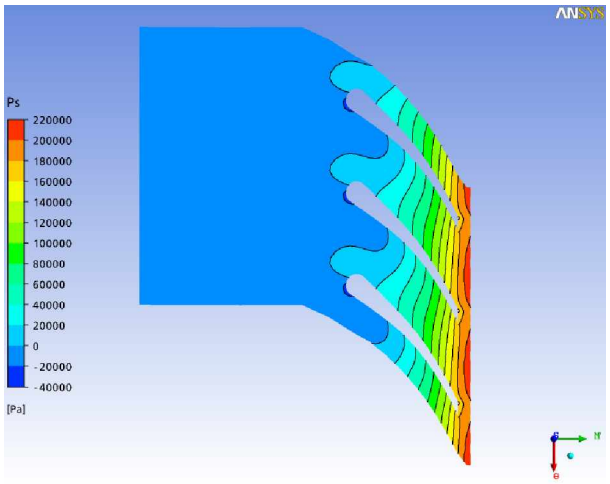

Fig 6.4 Distribution of static pressure at 50 span

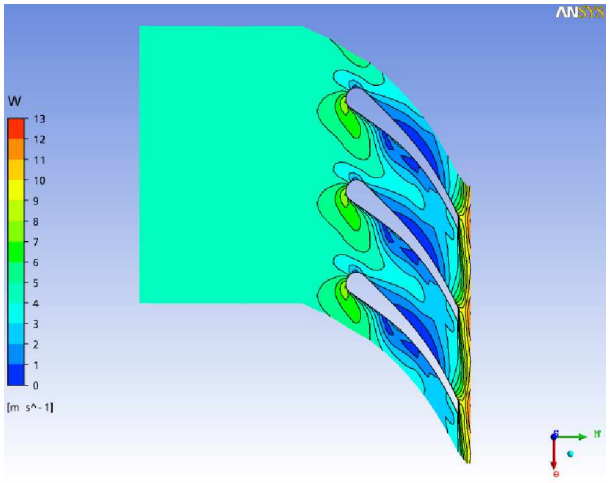

Fig 6.5 Distribution of relative velocity at 50 span

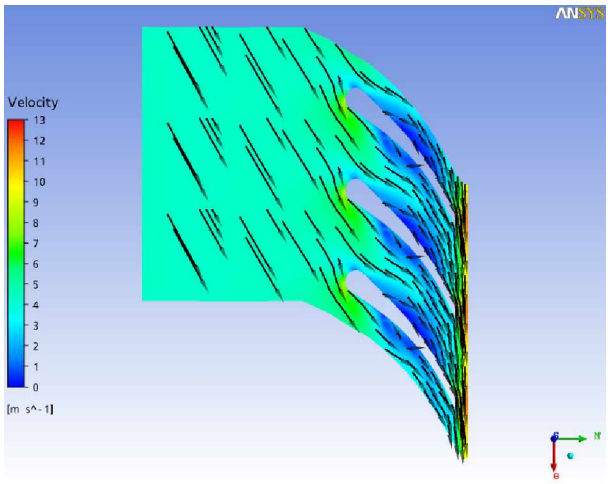

Fig 6.6 Relative velocity vector at 50 span

6.2.3 Flow pattern at leading and trailing edges

The effects on the flow at the leading and trailing edge are shown in the following figures. Minimum pressure is observed at the suction side of the leading edge. Pressure is higher towards the pressure side and it decreases towards the suction side of the impeller as shown if fig [6.7]. This is because the flow separation takes place at the inlet towards the suction side of the blade. There is large variation in the values of relative velocities at the leading edge shown in fig [6.8]. This is also because of the flow separation which is taking place at the leading edge towards the suction side of the impeller. Similarly, the fig [6.9] and fig [6.10] shows the variations at the trailing edge. Fig [6.11] shows the velocity streamlines at the trailing edge which shows that how the flow leaves the blades of the impeller.

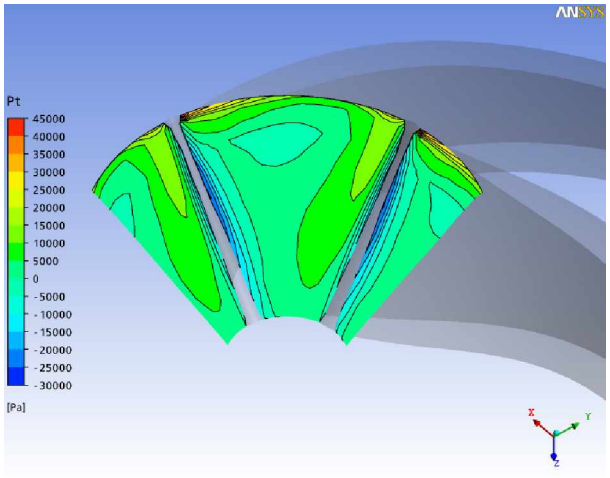

Fig 6.7 Distribution of total pressure at blade leading edge

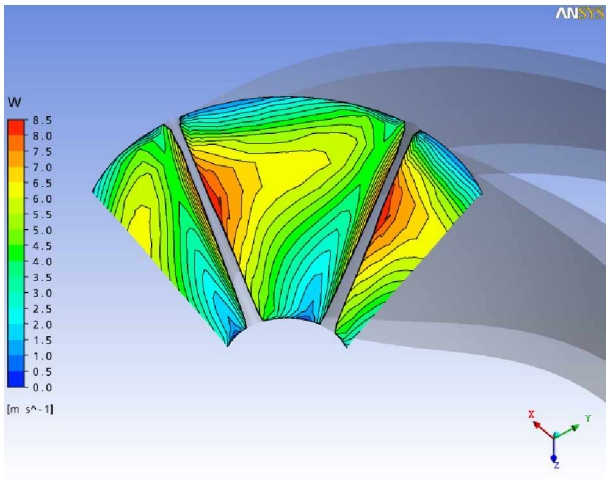

Fig 6.8 Distribution of relative velocity at blade leading edge

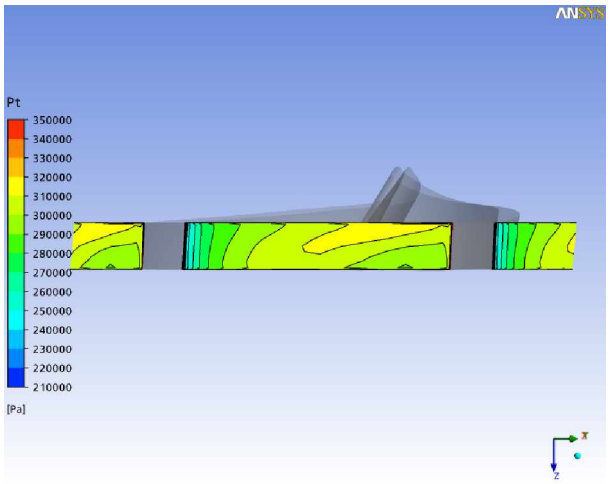

Fig 6.9 Distribution of total pressure at blade trailing edge

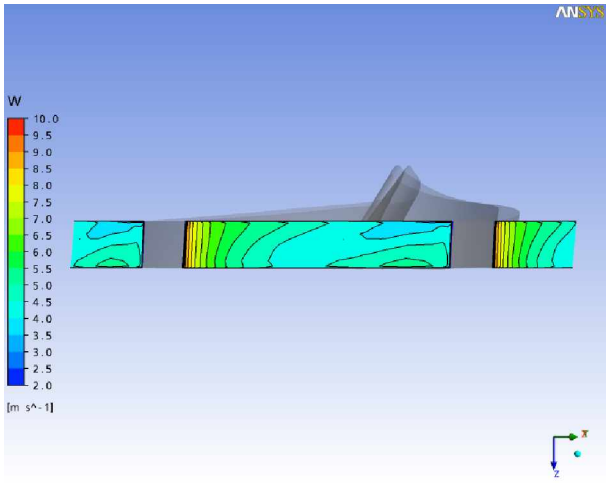

Fig 6.10 Distribution of relative velocity at blade trailing edge

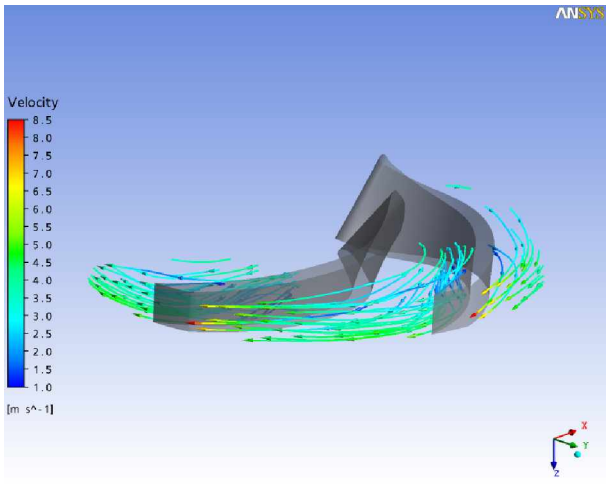

Fig 6.11 distribution of velocity streamline at trailing edge

6.2.4 Blade loading at pressure and suction side

The blade loading of pressure and suction side are drawn at three different locations on the blade at the span of 20, 50 and 80 from hub towards the shroud. The pressure loading on the impeller blade is shown in fig [6.12]. Pressure load on the impeller blade is plot along the streamwise direction. The pressure difference on the pressure and suction sides of the blade suggests that the flow inside the impeller experiences the shearing effects due to the pressure difference on blade-to-blade passage wall.

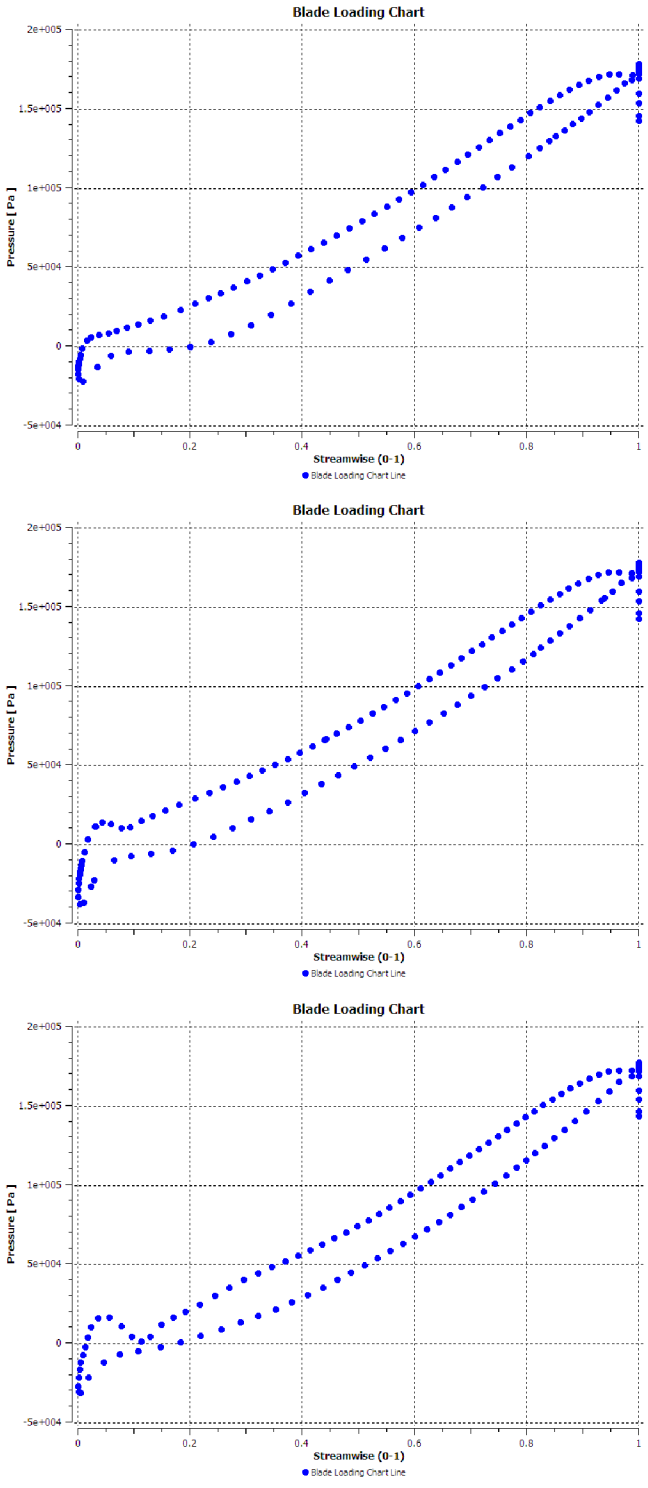

Fig 6.12 Blade loading at 20, 50 and 80 span

6.2.5 Variation of flow rate on pressure

The effects of flow rate on the pressure inside the impeller passage along the streamwise direction are observed by comparing the results obtained from the simulation at different flow rates. For this purpose, simulations are conducted on this pump impeller at eight different flow rates. Fig [6.13] shows the flow rate effects on the pressure distribution on the impeller blade. For all the blades, the biggest pressure fluctuation on the impeller blade is observed at the trailing edge. It is observed that the flow rate has significant effect on the pressure fluctuation at the trailing edge. It is also observed that pressure increases with decreasing flow rate. The variation in pressure is shown along the streamline from inlet to the outlet with different flow rates. The pressure for the minimum flow rate is found maximum at the outlet of the impeller and wise versa.

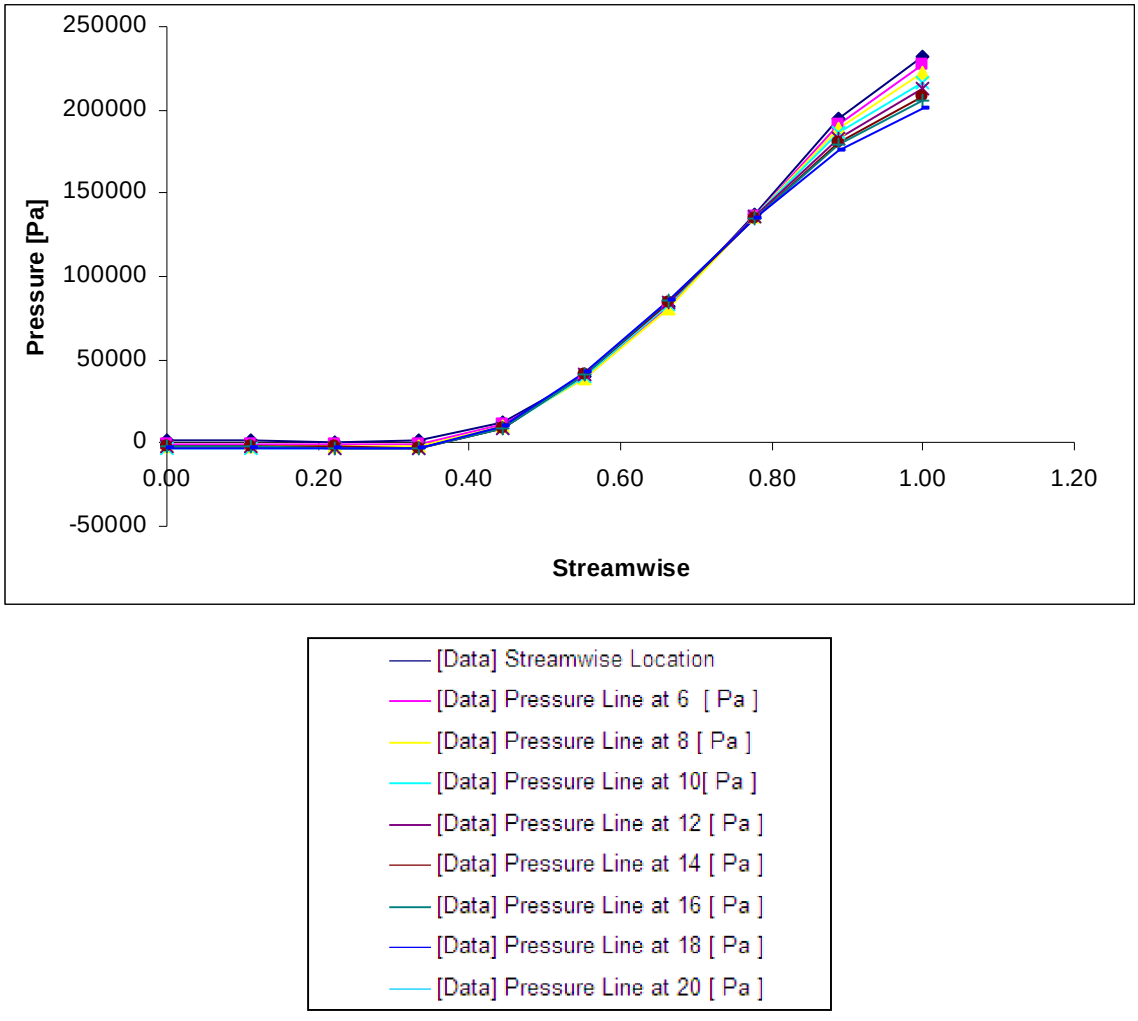

Fig 6.13 Pressure fluctuation from inlet to outlet at streamwise location.

6.2.6 Flow pattern in the impeller

The variation in the flow pattern with the change in flow rate is shown in the fig [6.14] below. At low flow rates strong recirculation of flow takes place in suction side of the blade, whereas the flow in pressure side is smooth. But as the flow rate increases the flow separation along the pressure side of the impeller blade takes place, which results in the recirculation of flow in the pressure side. The recirculation in the suction side of the impeller blade decreases as the flow rate increases. Increased flow velocity can be

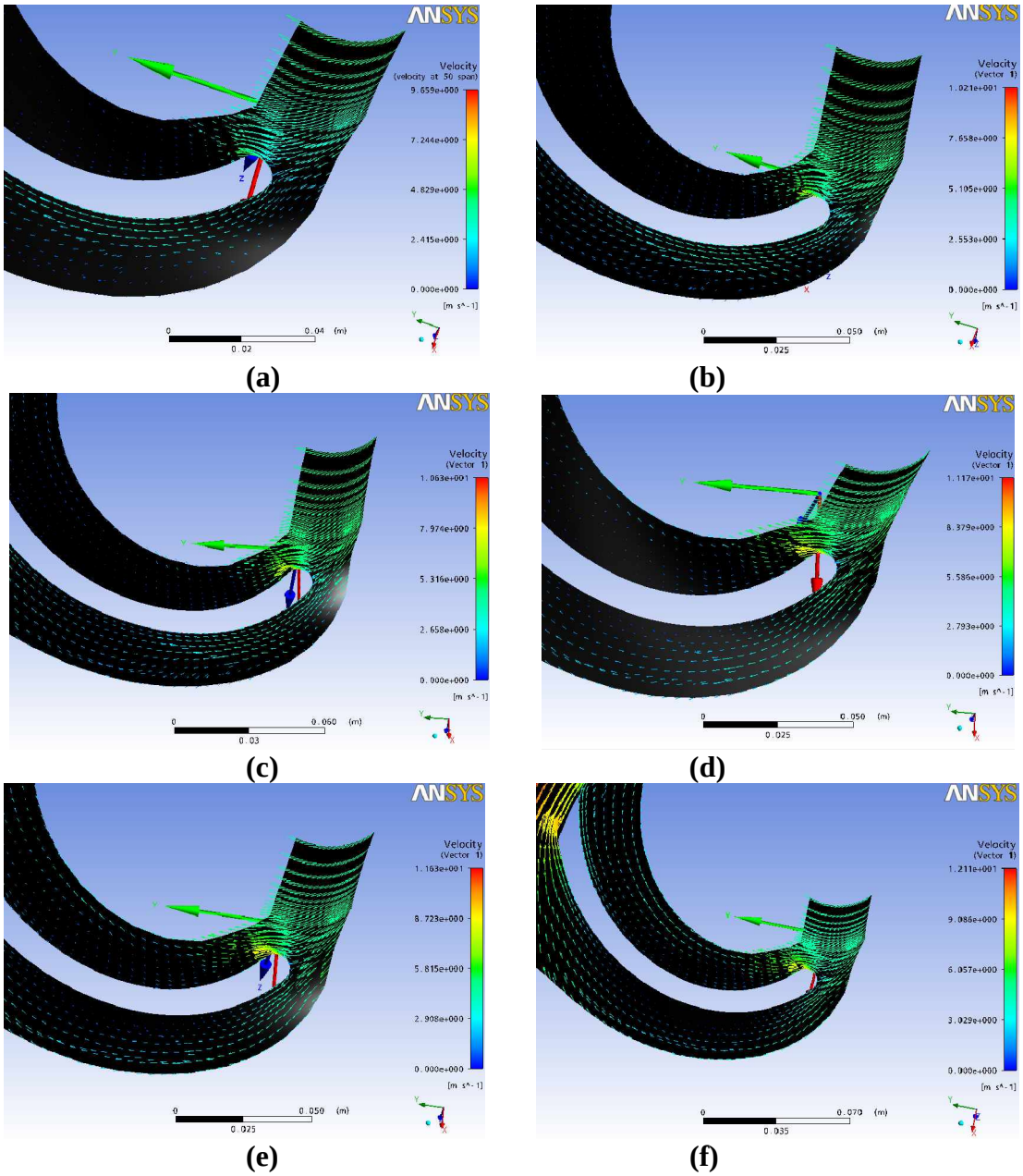

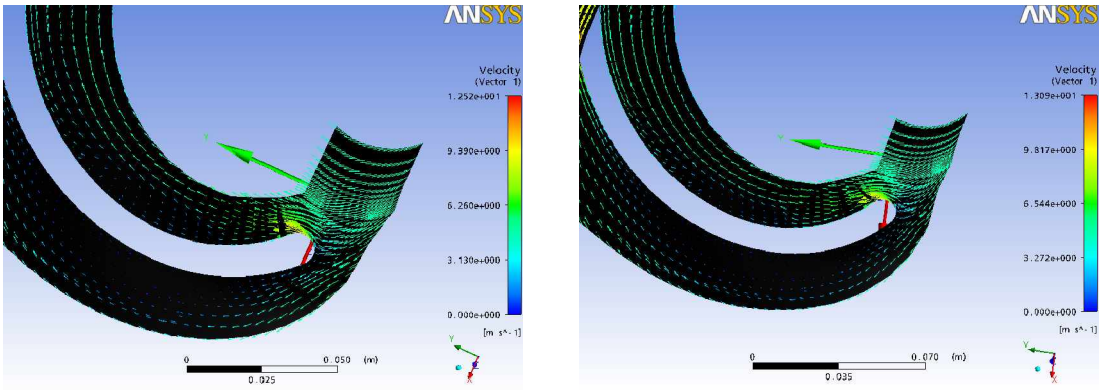

(g) **(h)**

Fig 6.14 Variation in flow with changing flow rate

observed at the blade inlet due to the blockage of the flow towards the suction side of the impeller blade. It further increases with increase in the flow rate of the impeller passage in the pump.

6.3 PERFORMANCE CURVES

6.3.1 Variation of performance with flow rate for water

The fig [6.15] shows the head-flow curve for water as fluid in the impeller flows at different flow rates. It is found that the head of pump decreases gradually as the flow rate in the pump increases. The variation of input power required with the changing flow rate is shown in fig [6.16]. The required power increases with the increase in the flow rate. The variation of efficiency with changing flow rate of water as fluid in the pump impeller is also shown in the fig [6.17].

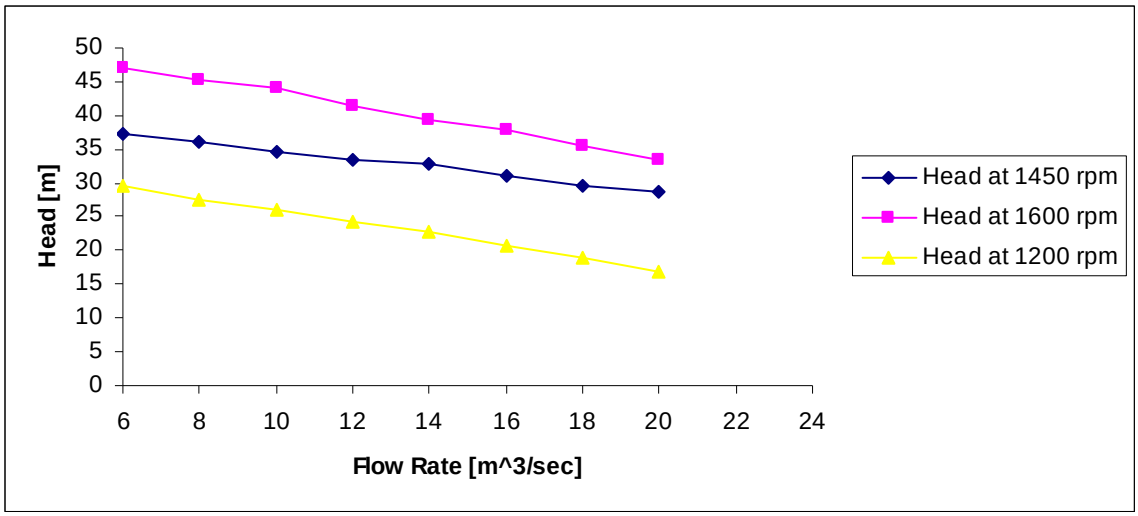

Fig 6.15 Head vs flow rate for water

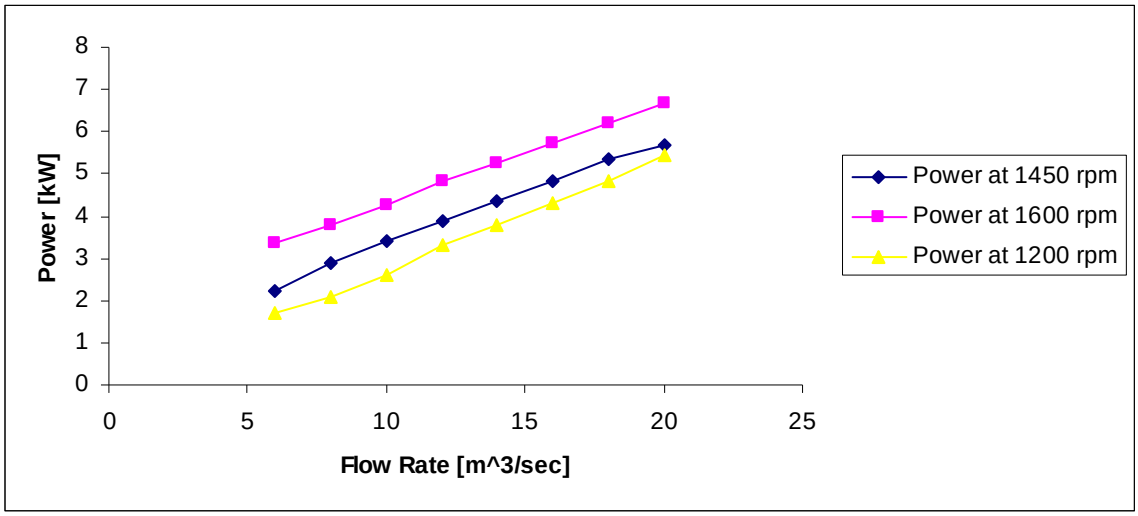

Fig 6.16 Power vs flow rate for water

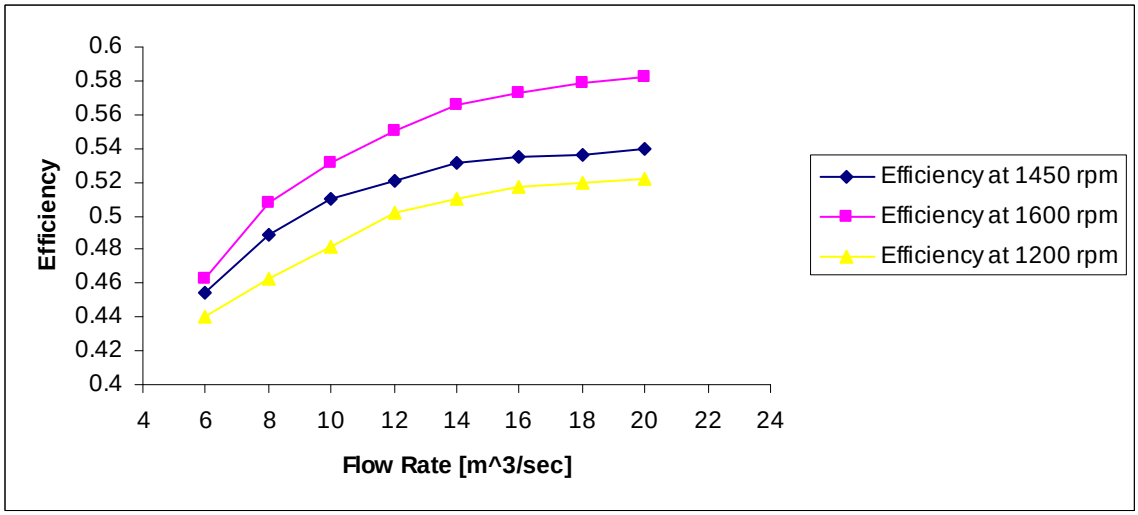

Fig 6.17 Efficiency vs flow rate for water

6.3.2 Variation of performance with changing concentration of solid

The effect of adding solid particles in the fluid are studied. It is observed that the head of the pump decreases with increasing the concentration of solids in the fluid. Though, the variation in the head of the pump is not very high for different concentrations as the concentration of the sand is low in the fluid. Generally, the head of the pump decreases appreciably as the concentration of the sand will increase in the fluid. Similarly, the efficiency of the pump decreases with increasing concentration of solid particles.

Whereas the power required for the pump increases with the increasing concentration of the solid particles. The variation of head, power and efficiency at 2%, 5%,10% and 15% solid concentration in the fluid are shown in fig [6.18], fig [6.19] and fig [6.20] respectively.

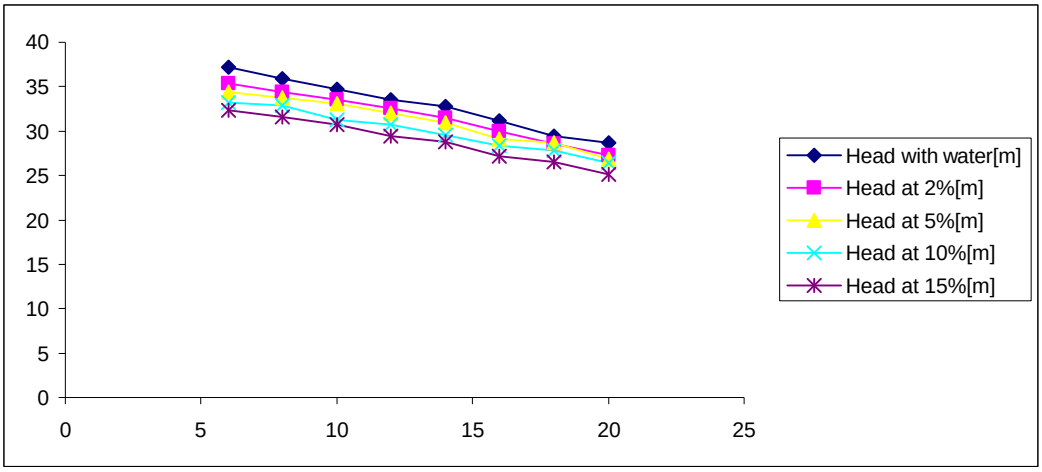

Fig 6.18 Head vs flow rate for water with sand at different conc.

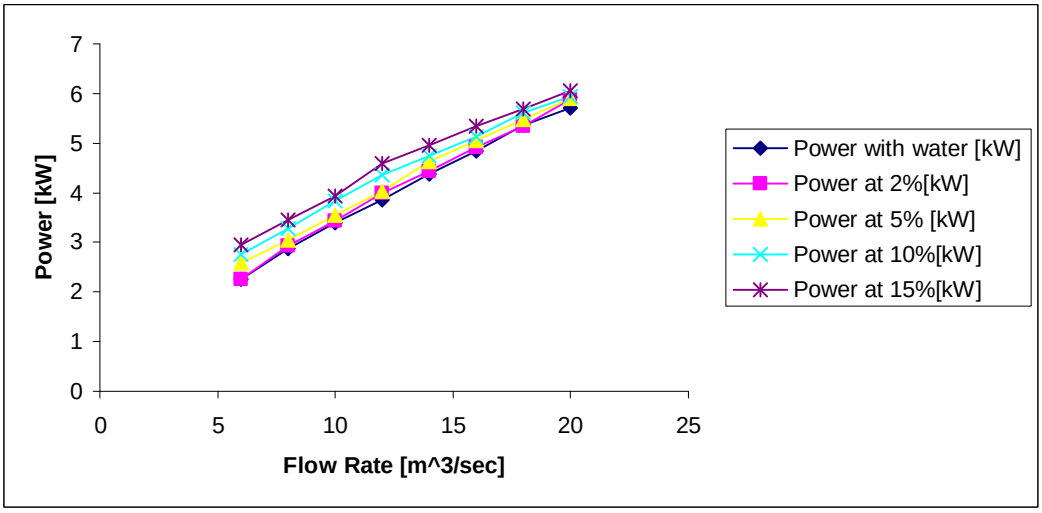

Fig 6.19 Power vs changing flow rate at different concentration of sand

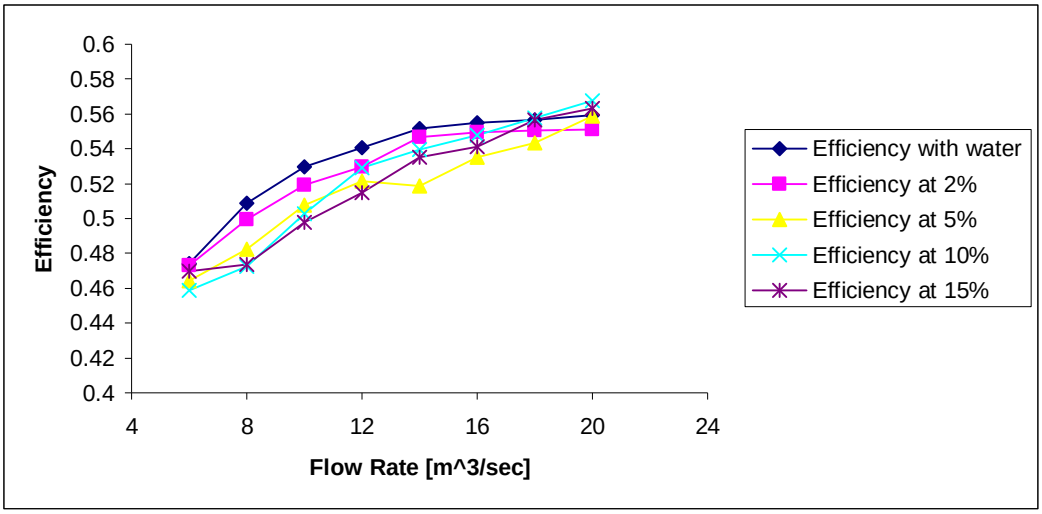

Fig 6.20 Power vs changing flow rate at different concentration of sand

6.3.3 Effect of speed on the head of the pump

The effects of change in speed of the pump on the head are simulated and the results are shown in the fig [6.21]. The head of the pump varies linearly, ie with increase in the speed of the pump the value of head increases.

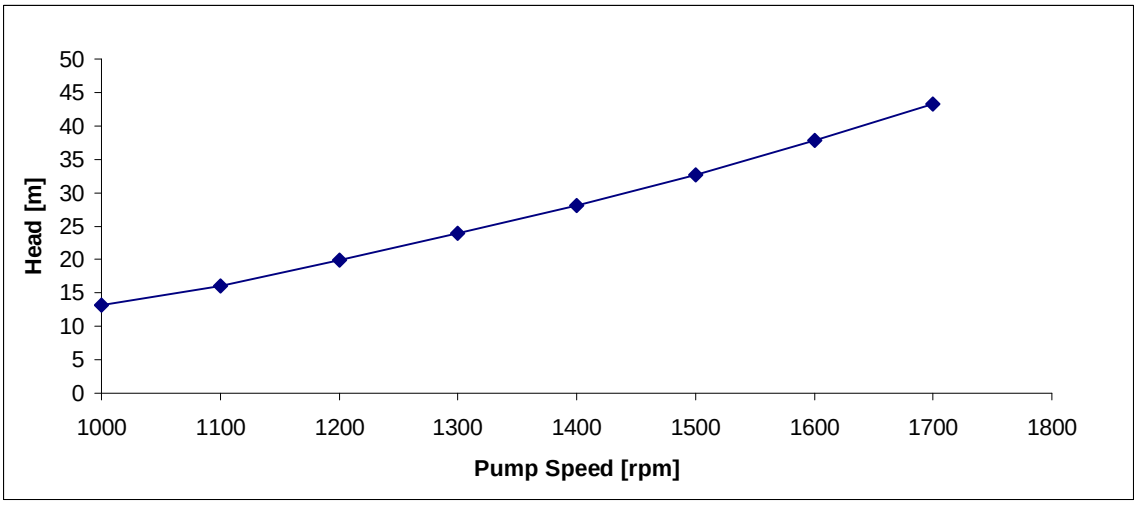

Fig 6.21 Variation in head with changing pump speed

6.3.4 Effect of concentration on the head at different speeds of the pump

As the speed of the pump increases the head increases for the same concentration, but as the concentration of solid increases there is decrease in the head of the pump. This is shown in fig [6.22].

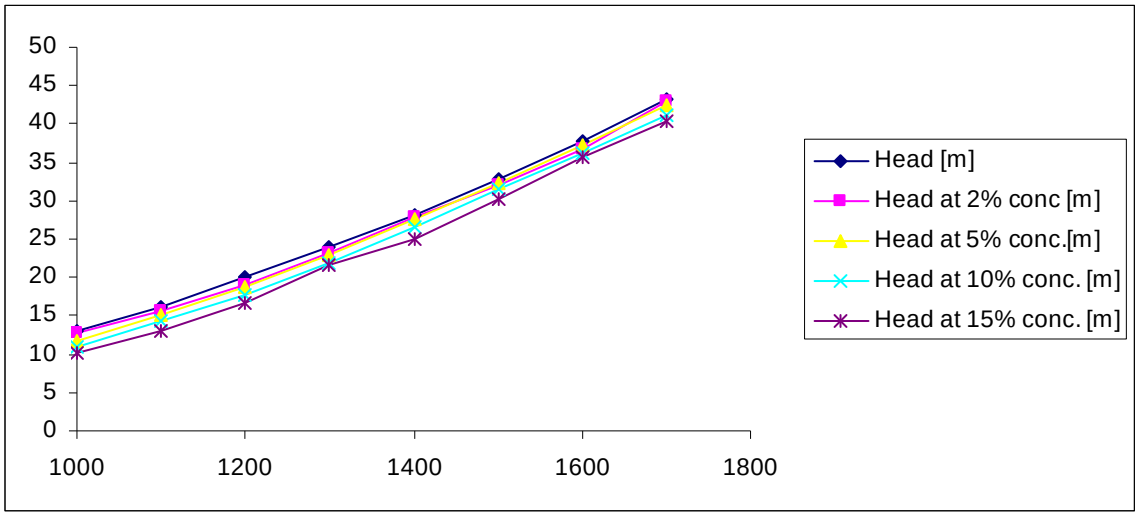

Fig 6.22 Variation in head with changing speed at different concentrations.

6.3.5 Pressure variation

The value of pressure inside the impeller passage from inlet to the outlet, increases as the speed increases. Though the variation in the pressure is appreciable in all around the passage of the blade, the maximum effect can be seen at the trailing edge of the impeller blade as shown if fig [6.23].

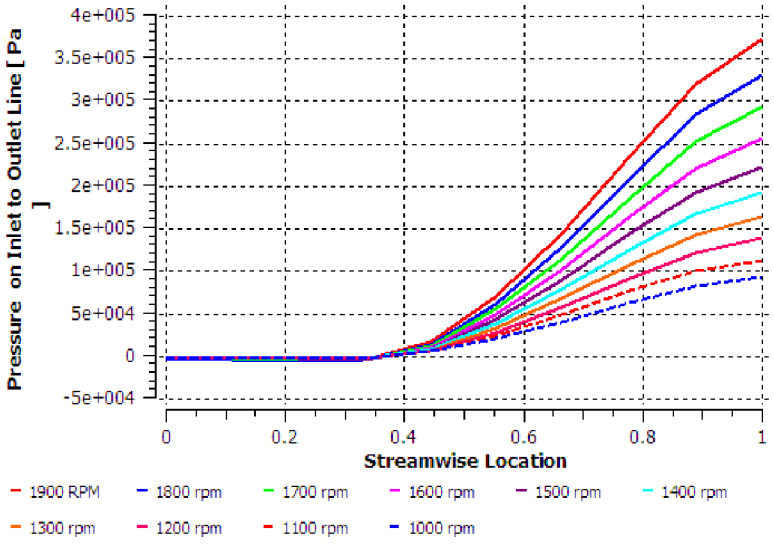

Fig 6.23 Pressure variation from inlet to outlet with changing speed

CHAPTER 7

CONCLUSION AND SCOPE FOR FUTURE WORK

A numerical model of an impeller has been successfully generated and the complex internal flow fields are investigated by using the Ansys-CFX code. Simulation results are obtained at different flow rates, speeds and concentrations. The internal flow is not quite smooth in the suction and pressure side of the blade due to non tangential inflow conditions which results in the flow separation at the leading edge. The pressure increases gradually along the streamwise direction. The regions in the impeller experiencing the largest pressure were located at the outlet. At low flow rates strong recirculation of flow takes place in suction side of the blade, whereas the flow in pressure side is smooth. But as the flow rate increases the flow separation along the pressure side of the impeller blade takes place, which results in the recirculation of flow in the pressure side. The recirculation in the suction side of the impeller blade decreases as the flow rate increases. Increased flow velocity can be observed at the blade inlet due to the blockage of the flow towards the suction side of the impeller blade. It further increases with increase in the flow rate of the impeller passage in the pump.

Pump performance curves generated shows good agreement with the open literature. It is concluded that with the increase in the flow rate head decreases linearly. There is further decrease in the head as sand particles are added into the fluid. The input power of the pump increases with increase in the flow rate as well as with the increasing concentration of the sand in the fluid. Whereas, in the case of the efficiency, there is not much of the change for changing flow rate at different concentrations. It is also concluded that the head of the impeller increases with increase in the speed of the impeller. And same decreasing trend is seen when the concentration of the fluid is changed.

Scope for future work

- Wear analysis of the impeller can be done with different slurries.
- Volute casing flow structure can be analyzed.

- Ø Same CFD method can be applied for calculating velocity and pressure in other turbo machinery components.

Further work can be taken up to see the effect of variation in clearance gaps like side spacing between impeller and casing, volute tongue clearance etc. on performance and wear characteristics of slurry pumps.

REFERENCES

1. Miner, S. M., (1997), "3-D Viscous Flow Analysis of an Axial Flow Pump Impeller" International Journal of Rotating Machinery, Volume 3, No. 3, pp 153-161.
2. Murugan, D. M., Tabakoff, W. and Hamed, A., (1997), "Flow Measurements and Flow Analysis in the Exit Region of a Radial Turbine" International Journal of Rotating Machines", Volume 3, No. 2, pp 93-105.
3. Sellgren, A., Addie, G. and Yu, W. C., (1999), "Effects of non-newt0nia.n mineral suspensions on the performance of centrifugal pumps" International Journal of Mineral Processing and Extractive Metallurgy Review, volume 20, No. 1, pp 239 – 249.
4. Majidi, K. and Siekmann H. E., (2000), "Numerical calculation of secondary flow in pump volute and circular casings using 3D viscous flow techniques" International Journal of Rotating Machinery, Volume 6, No. 4, pp 245-252.
5. Ogut, A. and Pastor, D. G., (2000), "Simulation of flow in turbopump vaneless and vaned diffusers with fluid section" International Journal of Rotating Machinery, Volume 6, No. 1, pp 57-65.
6. Medvitz, R. B., Kunz, R. F., Boger, D. A., Lindau, J. W., and Yocum, A. M., (2001), "Performance analysis of cavitating flow in centrifugal pumps using multiphase CFD" Proceedings of ASME Fluids Engineering Conference May 29 - June 1, 2001, New Orleans, Louisiana.
7. Gandhi, B. K., Singh, S. N. and Seshadri, V., (2001), "Performance characteristics of centrifugal slurry pumps" Journal of Fluids Engineering, Volume 123, pp 271-280.
8. Engin, T. and Gur, M., (2001), "Performance characteristics of a centrifugal pump impeller with running tip clearance pumping solid-liquid mixtures" American Society of Mechanical Engineering, volume 123, pp 532-538.
9. Miner, S, M., (2001), "3-D Viscous flow analysis of a mixed flow pump impeller" International Journal of Rotating Machinery, Volume 7, pp 53—63.

10. Kouidri, S., Bakir, F. and Rey, R., (2002), “Mass flow rate measurement in heterogeneous diphasic flows by using the slurry pumps behavior” Flow Measurement and Instrumentation, volume 13, pp 45–51.
11. Baun, D. O. and Flack, R. D., (2003), “Effects of volute design and number of impeller blades on lateral impeller forces and hydraulic performance” International Journal of Rotating Machinery, volume 9, pp 145–152.
12. Zhou, W., Zhao, Z., Lee, T. S., and Winoto, S. H., (2003), “Investigation of flow through centrifugal pump impellers using computational fluid dynamics” International Journal of Rotating Machinery, volume 9, pp 49–61.
13. Kato, C., Mukai, H., and Manabe, A., (2003), “Large-eddy simulation of unsteady flow in a mixed-flow pump” International Journal of Rotating Machinery, volume 9, pp 345–351.
14. Nursen, E. C., and Ayder, E., (2003), “Numerical calculation of the three-dimensional swirling flow inside the centrifugal pump volutes” International Journal of Rotating Machinery, volume 9, 247–253.
15. Kochevsky1, A. N., Nenya, V. G., (2004), “Contemporary approach for simulation and computation of fluid flows in centrifugal hydromachines” International Journal of Physics, volume 36, pp 167-186.
16. Hergt, P., Meschkat, S. and Stoffel, B., (2004), “The flow and head distribution within the volute of a centrifugal pump in comparison with the characteristics of the impeller without casing” Journal of Computational and Applied Mechanics, Volume 5, pp 275-285.
17. Xu, C. and Muller, M., (2005), “Development and design of a centrifugal compressor volute” International Journal of Rotating Machinery, volume 3, pp 190–196.
18. Asuaje, M., Bakir, F., Kouidri, S., Kenyery, F., and Rey, R., (2005), “Numerical modelization of the flow in centrifugal pump: volute influence in velocity and pressure fields” International Journal of Rotating Machinery, volume 3, pp 244–255.

19. Ogata, S., Kimura, A., and Watanabe, K., (2006), “Effect of surfactant additives on centrifugal pump performance” American Society of Mechanical Engineering, volume 128, pp 174-198.
20. Shujia, Z., Baolin, Z., Qingbo, H., and Xianhua, L., (2006), “Virtual performance experiment of a centrifugal pump” Proceedings of the 16th International Conference on Artificial Reality and Telexistence, pp 243-254.
21. González, J., and Santolaria, C., (2006), “Unsteady flow structure and global variables in a centrifugal pump” Journal of Fluids Engineering, volume 128, pp 937-946.
22. Anagnostopoulos, J. S., (2006), “Numerical calculation of the flow in a centrifugal pump impeller using cartesian grid” International Conference on Applied and Theoretical Mechanics, Venice, Italy, pp 134-154.
23. Min-Guan, Y., Liu, D., and Dong, X., (2007), “Analysis of turbulent flow in the impeller of a chemical pump” Journal of Engineering Science and Technology volume 2, No. 3, pp 218 – 225.
24. Iancu, F., John, T., and Steven S., (2007), “Numerical analysis of blade geometry generation techniques for centrifugal compressors” International Journal of Rotating Machinery Volume 23, Article ID 48683, pp56-76.
25. Spence, R., Amaral-Teixeira, J., (2007), “Investigation into pressure pulsations in a centrifugal pump using numerical methods supported by industrial tests” Computers & Fluids, Article in Press.
26. Feng, J, Benra, F. K., and Dohmen, H. J., (2007), “Numerical investigation on pressure fluctuations for different configurations of vaned diffuser pumps” International Journal of Rotating Machinery, volume 27, pp 110-127.
27. Hofmann, M., Stoffel, B., Coutier-Delgosha, O., Fortes-Patella, R., Reboud, J. L., (2007), “Experimental and numerical studies on a centrifugal pump with 2d-curved blades in cavitating condition” CAV 2001 california institute of technology pasadena, california, usa 20-23 june, 2001.
28. PULLUM, L., GRAHAM, L.J.W. and RUDMAN, M., (2007), “Centrifugal pump performance calculation for homogeneous and complex heterogeneous

suspensions" The 17th International Conference on the Hydraulic Transport of Solids.

29. Younsi, M., Bakir, F., Kouidri, S., and Rey, R., (2007), "Influence of impeller geometry on the unsteady flow in a centrifugal fan: numerical and experimental analyses" International Journal of Rotating Machinery, Volume 07, Article ID 34901, 10 pages.

30. Younsi, M., Kergourlay, G., Bakir, F., and Rey, R., (2007), "Influence of splitter blades on the flow field of a centrifugal pump: test-analysis comparison" International Journal of Rotating Machinery, Volume 07, Article ID 85024, 13 pages.

31. Cheah, K.W., Lee, T. S., Winoto, S. H., and Zhao, Z.M., (2007), "Numerical flow simulation in a centrifugal pump at design and off-design conditions" International Journal of Rotating Machinery, Volume 27, pp 238-254.

Bibliography

32. Stepanoff, A. J., (1958), "Centrifugal and axial flow pumps theory design and application", 2nd ed, John wilay and sons, New York.

33. Stepanoff, A. J., (1965), **"**Pumps and blowers and two phase flow two-phase flow", John wilay and sons, New York.

34. Vasandani, V. P., (1993), "Hydraulic machines theory and design", 10th edition, Khanna Publishing house, New Delhi.

35. Ghoshdastidar, P. S., (1998), "Computer simulation of flow and heat transfer", Tata McGraw-Hill, New Delhi.

36. Kanetkar, Y. P., (2002), "Let us C", BPB publications, New Delhi.

37. Balagurusamy, E., (2005), "Programming in C#", Tata McGraw-Hill, New Delhi.

38. ANSYS CFX-Manual, (2006), Published by, ANSYS CFX, Release 11.0, December, 2006, ANSYS, Inc.

ANNEXURE I

PROGRAM FOR DESIGN OF CENTRIFUGAL PUMP

```
#include<stdafx.h>
#include<iostream>
using namespace std;
double a,b,c,u1;
void fn_Roots()
{
	double D = (b*b-4*a*c);
	if(D>=0)
	{
		double x1 = (-b+sqrt(D))/(2*a);
		double x2 = (-b-sqrt(D))/(2*a);
		if(x1>=0)
		{
			u1=x1;
		}
		if(x2>=0)
		{
			u1=x2;
		}
	}
	if(D<0)
		cout<<"\nEquation has imaginary roots"<<endl;
}
void main()
{
	//Enter the input parameters//
	double H,Q,p,N,Ns,Pin,P;
```

```
double  Oeff,Pw,Heff,Meff,Veff,pi=3.1415;
double theta=3.143*22/180,g=9.81,C1m,beta1;
double Q1,De,Ca,B1,b1,b2,a1,a2,a3,Beta2,C2,C3,u2,D1,Dh,Hr,C2m,w,dH,beta;
double T,Dsh,D2,D,b0,Ts,Cl,G1;
double phi,sai,Hs,w1,s1,r1;
double R,R1,dr=0.002;
int             z;
const double    r=1000;                 //Density of water
const double    s=25;                   //Shear stress of the shaft
const double    sigma=1.1;              //Varies from 0.9-1.1
const double    tow=1.05;               //Varies from 1.05-1.1
const double    k=0.84;                 //Varies from 0.75-0.85
const double    beta3=17.5*3.1415/180;
                                        //H=Head
                                        //Q=Flow Rate
                                        //p=N*sqrt(Q) term used in
                                        calculation of specific speed
                                        //Ns=Specifc speed
cout<<"**************************************************************
*****************"<<endl;
cout<<"PROGRAM FOR THE INPUT PARAMETERS FOR THE DESIGN OF
CENTRIFUGAL PUMP IMPELLER"<<endl;
cout<<"**************************************************************
*****************";
cout<<"\nEnter the value of desired head of the pump (meters):  "<<"\t";
cin>>H;
cout<<"\nEnter the value of desired flow rate (m^3 per sec):  "<<"\t";
cin>>Q;
cout<<"\nEnter the value of desired speed of the pump (rpm):  "<<"\t";
cin>>N;
cout<<"\nEnter the value of overall efficiency of pump (%):  "<<"\t";
```

```
//Take the value from the Stepanoff's curves
cin>>Oeff;
cout<<"\nEnter the value of Vol. efficiency of the pump(%):  "<<"\t";
//Normally varies from 0.85 to 0.98
cin>>Veff;
cout<<"**********************************************************************
**********";
cout<<"\nCONSTANTS USED IN THE CALCULATION \n"       ;
cout<<"**********************************************************************
**********";
cout<<"\n\nDensity of water(r):"<<"\t\t\t\t"<<r<<" kg/cubic metre";
cout<<"\nAccleration due to gravity(g):"<<"\t\t\t"<<g<<" metre per sec sqr";
cout<<"\nShear stress of the shaft in MPa(s):"<<"\t\t\t"<<s;
cout<<"\nsigma:"<<"\t\t\t\t\t\t"<<sigma;
cout<<"\ntow:"<<"\t\t\t\t\t\t"<<tow;
cout<<"\nk:"<<"\t\t\t\t\t\t"<<k;
cout<<"\n**********************************************************************
**********";
cout<<"\nRESULTS OF THE GIVEN INPUT"<<"\n";
cout<<"\n**********************************************************************
*           **********";
p=N*sqrt(Q);
Ns=p/pow(H,0.75);
//Calculation of specific speed
cout<<"\nSpecfic speed of the pump is"<<": "<<"\t\t\t"<< Ns <<"\n\n";
//The values of Ns and Q are used to get the value for overall efficiency from the
Stepanoffs curve
Heff=1-(0.66*(1-Oeff));                 //Using Wislicenus formula for finding
hydraulic efficiency
cout<<"\nHydrualic efficiency of the pump :  "<<"\t\t\t"<<Heff<<"%"<<"\n\n";
Meff=(Oeff)/(Heff*Veff);
```

```
cout<<"\nMechanical Efficiency of the pump: "<<"\t\t\t"<<Meff<<"%"<<"\n\n";
P=(r*g*Q*H)/(745*Oeff);
Pin=1.15*P;                              //Keeping the margin of 15%
Pw=Pin*745;
cout<<"\nInput power of the pump:   "<<"\t\t\t\t"<<Pin<<" HP "<<endl;
cout<<"\nInput power of the pump: "<<"\t\t\t\t"<<Pw<<" Watts "<<endl;

//Calculation of Shaft diameter
T=Pw*60*1000/(2*pi*N);
cout<<"\nTorque: "<<"\t\t\t\t\t\t"<<T<<endl;
D=16*T/(pi*s);
Dsh=pow(D,0.333333);
cout<<"\nDiameter of the Shaft:  "<<"\t\t\t\t"<<Dsh<<" mm"<<endl;

        Q1=Q+(Q*0.08);
        a1=sigma*sigma*tan(beta3)*tan(beta3);
        a2=tow*tow*k;
        a3=a1/a2;
        a=pow (a3,0.3333);
        b1=N*N*Q1;
        b=pow (b1,0.3333);
        Ca=0.152*a*b;                                    //Axial velocity

        cout<<"\nAxial velocity: "<<"\t\t\t\t\t"<<Ca<<endl;
        De=sqrt((4*Q1)/(pi*k*Ca));                       //Dia of eye
        cout<<"\nEye diameter: "<<"\t\t\t\t\t\t"<<De<<" meters"<<endl;
        D2=0.95*De;
        cout<<"\nInlet blade diameter: "<<"\t\t\t\t\t"<<D2<<" meters"<<endl;
        C3=Ca*1.05;
        C2=1.1*C3;
        Dh=1.2*Dsh;
```

```
cout<<"\nHub diameter: "<<"\t\t\t\t\t\t"<<Dh<<" mm"<<endl;
b2=(Q1)/(pi*D2*C3);
cout<<"\nWidth at inlet: "<<"\t\t\t\t\t"<<b2<<" meters"<<endl;
u2=(pi*D2*N)/(60);
cout<<"\nInlet blade velocity: "<<"\t\t\t\t\t"<<u2<<" meter per
second"<<endl;                          //Inlet blade velocity
beta=atan(C2/u2);
Beta2= beta * 180/3.1415;
cout<<"\nInlet blade angle"<<"\t\t\t\t\t"<<Beta2<<" degree"<<endl;
                                        //Inlet blade angle
double pq=0.32;                         //Varies from 0.28 to 0.32
double ang=25*3.1415/180;
double outang=ang*180/3.1415;           // Value recomended by
stefnoff's
Hr=((1+pq)*H)/Heff;
C2m=1.1*C3;
                                        // meridional flow velocity
C1m=0.9*C2m;
a=1;
b=-(C2m)/(tan(ang));
c=-(Hr*9.81);
fn_Roots();
//Call of function for calculation of roots of quadratic equation
cout<<"\nOutlet blade velocity: "<<"\t\t\t\t\t"<<u1<<" meters per
sec"<<endl;
D1 = (60*u1)/(pi * N);
//CALCULATION OF NUMBER OF BLADES
cout<<"\nOutlet diameter of blade: "<<"\t\t\t\t"<<D1<<" meters"<<endl;
z=2*pi*sin(theta)*((D2+D1)/(D1-D2));
cout<<"\nNumber of blades: "<<"\t\t\t\t\t"<<z+1<<endl;
B1=(Q1)/(pi*D1*C1m);
```

```
cout<<"\nBreadth at outlet of blade"<<"\t\t\t\t"<<B1<<" meters"<<endl;

double t1=0.3,t2=1.2;                                    //
CALCULATION OF NPSH
w=C3/sin(beta3);
dH=((t1*w*w)+(t2*C3*C3))/(2*g);
cout<<"\nNPSH Required is:"<<"\t\t\t\t\t"<<dH<<endl;
cout<<"\nOutlet blade angle: "<<"\t\t\t\t\t"<<outang<<" degree"<<"\n\n";

cout<<"**************************************************
**********************";
cout<<"\nCALCULATION OF VOLUTE CASING"<<endl;

cout<<"**************************************************
**********************"<<endl;

Hs=H/Heff;
w1=2*pi*N/60;
Ts=0.003;                                  // thickness of shroud
Cl=0.002;                                  // clearence
sai=(360*g*H)/(Q1*w1*Heff);
b0=(2*B1)+(2*Ts)+(2*Cl);                   //Width of volute
cout<<"\nWidth of the volute:"<<"\t\t\t\t\t"<<b0<<endl;
r1=D1/2;
s1=r1+r1/30;
R=s1+0.01;
R1=R+0.50;
G1=(-1.154*s1)+b0;
cout<<"\n Increasing Radius and angles of
volute"<<"\t\t"<<"Radius"<<"\t\t"<<"Angle"<<"\n\n";
while((R1>R)||(R1==R))
```

```
{

        phi=sai*((1.154*(R-s1))+(G1*(log(R)-log(s1))));

        if (phi>=360)
        break;
        cout<<"\t\t\t\t\t\t"<<R<<"\t\t"<<phi<<endl;
        R=R+dr;
}
cout<<endl<<endl;


}
```

ANNEXURE II

OUTPUT OF THE PROGRAM

****

PROGRAM FOR THE INPUT PARAMETERS FOR THE DESIGN OF CENTRIFUGAL PUMP IMPELLER

****

ENTER THE VALUE OF DESIRED HEAD OF THE PUMP (METERS):	14.5
ENTER THE VALUE OF DESIRED FLOW RATE (M^3 PER SEC):	0.016
ENTER THE VALUE OF DESIRED SPEED OF THE PUMP (RPM):	1450
ENTER THE VALUE OF OVERALL EFFICIENCY OF PUMP (%):	0.46
ENTER THE VALUE OF VOL. EFFICIENCY OF THE PUMP (%):	0.92

****

CONSTANTS USED IN THE CALCULATION

****

DENSITY OF WATER(R):	1000 KG/CUBIC METER
ACCELERATION DUE TO GRAVITY (G):	9.81 METER PER SEC SQR
SHEAR STRESS OF THE SHAFT IN MPA(S):	25
SIGMA:	1.1
TOW:	1.05
K:	0.84

****

RESULTS OF THE GIVEN INPUT

****

SPECIFIC SPEED OF THE PUMP IS:	24.6832
HYDRAULIC EFFICIENCY OF THE PUMP:	0.6436%
MECHANICAL EFFICIENCY OF THE PUMP:	0.77688%
INPUT POWER OF THE PUMP:	7.63732 HP
INPUT POWER OF THE PUMP:	5689.8 WATTS
TORQUE:	37472.5
DIAMETER OF THE SHAFT:	19.6902 MM

AXIAL VELOCITY:	2.54876
EYE DIAMETER:	0.101375 METERS
INLET BLADE DIAMETER:	0.0963058 METERS
HUB DIAMETER:	23.6283 MM
WIDTH AT INLET:	0.021342 METERS
INLET BLADE VELOCITY:	7.3115 M/ SEC
INLET BLADE ANGLE	21.9318 DEGREE
OUTLET BLADE VELOCITY:	20.5262 METERS PER SEC
OUTLET DIAMETER OF BLADE:	0.270368 METERS
NUMBER OF BLADES:	5
BREADTH AT OUTLET OF BLADE	0.00767887 METERS
NPSH REQUIRED:	1.6492
OUTLET BLADE ANGLE:	25 DEGREE

****

CALCULATION OF VOLUTE CASING

****

WIDTH OF THE VOLUTE:	0.0253577	
INCREASING RADIUS AND ANGLES OF VOLUTE	RADIUS	ANGLE
	0.14969	65.1251
	0.15169	80.4393
	0.15369	96.4696
	0.15569	113.198
	0.15769	130.605
	0.15969	148.676
	0.16169	167.393
	0.16369	186.74
	0.16569	206.702
	0.16769	227.264
	0.16969	248.412
	0.17169	270.133
	0.17369	292.413